

UC Riverside

UC Riverside Electronic Theses and Dissertations

Title

Engineering Low-Dimensional Nanostructures Towards Flexible Electronics

Permalink

<https://escholarship.org/uc/item/3ck3m4g3>

Author

Byrley, Peter Samuel

Publication Date

2017

Copyright Information

This work is made available under the terms of a Creative Commons Attribution License, available at <https://creativecommons.org/licenses/by/4.0/>

Peer reviewed|Thesis/dissertation

UNIVERSITY OF CALIFORNIA
RIVERSIDE

Engineering Low-Dimensional Nanostructures Towards Flexible Electronics

A Dissertation submitted in partial satisfaction
of the requirements for the degree of

Doctor of Philosophy

in

Chemical and Environmental Engineering

by

Peter Samuel Byrley

June 2017

Dissertation Committee:

Dr. Ruoxue Yan, Chairperson

Dr. Nosang Myung,

Dr. Juchen Guo

Copyright by
Peter Samuel Byrley
2017

The Dissertation of Peter Samuel Byrley is approved:

Committee Chairperson

University of California, Riverside

ACKNOWLEDGEMENTS

I would like to thank my advisor, Dr. Ruoxue Yan, for all of her advice and support. Thank you for being patient with me especially when I was pursuing creative, crazy ideas that I couldn't exactly explain why I thought they would work. I came into these projects with little background knowledge and learned an extremely large amount in a short amount of time. I would also like to thank Dr. Ming Liu for all of his advice on creating and testing electrical devices. Even though I may not always have shown it, I appreciated your jokes.

I would like to thank my committee members Dr. Juchen Guo, Dr. Nosang Myung and former final committee member Dr. Elaine Haberer. In conversations I've had with you, you not only provided advice about the research presented here but also how to find information and use it effectively to do research.

Thank you to Sanggon Kim. Starting in the lab together, you were much more experienced than me and taught me much needed lab techniques that made me grow as a researcher. Yangzhi Zhu, Qiushi Liu, In Jun Park, and Xuezhi Ma, it was fun working together at times. I hope we taught each other things that will help our future careers.

Thank you to Dr. Ming Lee Tang for letting me use your thermal evaporator. It saved a lot on the costs that my project had. Thank you to Dr. Albert Wang and Qi Chen for letting me use your wire bonder. I am also in debt to the Central Facility for Advanced Microscopy and Microanalysis and the Center for Nano scale Science and Engineering for use of their facilities. Thank you also to the UCI Laboratory for Electron and X-Ray Instrumentation for use of their XPS facility and one-on-one training.

I would like to thank Dr. Charles Wyman and Dr. Phil Christopher. You provided personal advice that really changed my thoughts about graduate school research and what it means to earn a Ph.D. These conversations were extremely important to me and changed me as a person. I feel that they really helped shape my future career goals.

I would also like to thank graduate division including former dean Joseph Childers, current dean Dr. Kevin Esterling and assistant dean Kenneth Lai. The Grad Slam research competition really erased my “imposter syndrome” and made me realize that I am valued and have skills that will make me successful in the real world. You were extremely encouraging and I am really glad I got to know all of you. Thank you to the UC Office of the President staff that I met as well. It was a wild ride and you made it really fun.

Lastly, I would like to thank all of my close friends in the department including Glen Svenningsen, Pedro Piqueras, Abhishek Patri, Ninad Kothari and Brandon Simmons-Rawls. You helped make all of the late nights bearable and kept me focused on the light at the end of the tunnel.

Dedication

To my father Theodore Byrley,
You always told me I could do anything.

ABSTRACT OF THE DISSERTATION

Engineering Low-Dimensional Nanostructures Towards Flexible Electronics

by

Peter Samuel Byrley

Doctor of Philosophy, Graduate Program in Chemical and Environmental Engineering
University of California, Riverside, June 2017
Dr. Ruoxue Yan, Chairperson

Flexible electronics have been proposed as the next generation of electronic devices. They have advantages over traditional electronics in that they use less material, are more durable and have greater versatility in their proposed applications. However, there are a variety of types of devices being developed that have specific engineering challenges. This dissertation addresses two of those challenges. The first challenge involves lowering contact resistance in MoS₂ based flexible thin film transistor devices using a photochemical phase change method while the second addresses using silver nanowire networks as a replacement flexible electrode for indium tin oxide in flexible electronics.

In this dissertation, a scalable method was developed for making monolayer MoS₂ using ambient pressure chemical vapor deposition. These films were then characterized using spectroscopic techniques and atomic force microscopy. A photochemical phase change mechanism was then proposed to improve contact resistance in MoS₂ based devices. The central hypothesis is that the controllable partial transition from a semiconducting 2H to metallic 1T phase can be realized in monolayer TMDs through photo-reduction in the presence of hole scavenging chemicals. Phase-engineering in

monolayer TMDs would enable the fabrication of high-quality heterophase structures with the potential to improve carrier mobility and contact. Phase change as a result of the proposed photochemical method was confirmed using Raman spectroscopy, photoluminescence measurements, X-Ray photoelectron spectroscopy and other supporting data.

Gold coated silver nanowires were then created to serve as flexible nanowire based electrodes by overcoming galvanic replacement in solution. This was confirmed using various forms of electron microscopy. The central hypothesis is that a thin gold coating will enable silver nanowire meshes to remain electrically stable in atmosphere and retain necessary low resistance values and transparencies over time. It was shown that gold coated silver nanowire meshes could be created with sheet resistances comparable to indium tin oxide and outlast their bare silver nanowire counterparts in environments at 80 deg C.

CONTENTS

Acknowledgements	iv
Dedication	vi
Abstract.....	vii
List of Figures.....	xiii

CHAPTER 1

INTRODUCTION: LOW DIMENSIONAL FLEXIBLE ELECTRONICS

1.1 The development of flexible electronics	1
1.2 Flexible optoelectronic devices made from TMDs.....	2
1.2.1 The application of phase change for improving contact resistance in MoS ₂ based flexible transistors.....	5
1.3 The need for indium tin oxide alternatives in modern flexible electronics	11
1.4 Objectives of this work	12
1.5 Organization of this thesis	14
1.6 References	15

CHAPTER 2

CHEMICAL VAPOR DEPOSITION SYNTHESIS OF HIGH QUALITY MONOLAYER MOS₂

2.1 Introduction.....	21
2.2 Experimental details.....	22

2.3 Results and Discussion	28
2.3.1 Mechanically exfoliated MoS ₂	28
2.3.2 Raman spectroscopy of CVD produced MoS ₂	28
2.3.2 Photoluminescence.....	30
2.3.3 Atomic force microscopy.....	32
2.3.4 Transfer of MoS ₂ to other surfaces	33
2.4 References	35

CHAPTER 3

PHOTOCHEMICAL PHASE TRANSITION IN MONOLAYER MOS₂

3.1 Introduction.....	37
3.2 Experimental details.....	39
3.2.1 Creation of testing apparatus for use in phase change method	39
3.2.2 Time lapsed Raman characterization of MoS ₂	41
3.2.3 XPS characterization of the 1T phase	42
3.2.4 Photoluminescence mapping of MoS ₂ and atomic force microscopy .	43
3.2.5 Control experiments	44
3.2.6 Creation of electrical devices using 1T phase MoS ₂	46
3.2.7 Purely electrochemical method of phase change in monolayer MoS ₂	48
3.3 Results and Discussion	49
3.3.1 Raman characterization.....	49

3.3.2 XPS characterization.....	51
3.3.3 Photoluminescence mapping of MoS ₂ and atomic force microscopy .	53
3.3.4 Control experiments	56
3.3.5 Creation of electrical devices using 1T phase MoS ₂	58
3.3.6 Purely electrochemical method of phase change in monolayer MoS ₂ .	59
3.4 References.....	61

CHAPTER 4

AN EPITAXIAL, ULTRA-THIN GOLD COATING AS A BARRIER TO PREVENT OXIDATION OF SILVER NANOWIRES

4.1 Introduction.....	64
4.2 Experimental details.....	68
4.2.1 Creation of gold coated silver nanowires.....	68
4.2.2 Dropcasting of nanowires onto flexible substrates	69
4.2.2. Plasmonic nanowire welding	70
4.2.3. Press on filter method	71
4.2.4 Resistance measurements.....	73
4.3 Results and Discussion	76
4.3.1 Quality of gold coated silver nanowires	76
4.3.2 Dropcasting of silver nanowires onto flexible substrates	78
4.3.2 Plasmonic nanowire welding	79

4.3.3 Resistance measurements..... 79

4.4 References 84

CHAPTER 5

CONCLUSIONS

5.1 Summary 86

5.2 Suggestions for future work 88

List of Figures

Figure 1.1: A typical MOSFET. ⁵	2
Figure 1.2: (Left) Band structure of graphene. (Right) Band structure of monolayer MoS ₂ . ¹⁰	3
Figure 1.3: Contact resistance dominates resistance in TMD based devices. ²⁷	6
Figure 1.4: Two different phases of MoS ₂ , the 1T (Octahedral phase) and 2H (Trigonal prismatic phase). ⁶⁰	6
Figure 1.5: Li ⁺ ions intercalated between negatively charged MoS ₂ layers. ⁴¹	7
Figure 1.6: Simplified band structure diagram showing change from 2H to 1T MoS ₂	8
Figure 1.7: Simplified band structures for other TMDs. ⁵¹	9
Figure 1.8: Result of Re doped SEM scanning producing 1T MoS ₂ . ⁶⁰	10
Figure 2.1: The many routes of TMD synthesis. ²	21
Figure 2.2: (Left) Initial synthesis results using MoCl ₅ as a precursor. (Right) 3D model of inside CVD tube for system including conditions for synthesis.	23
Figure 2.3: Final successful CVD conditions for growth of large area MoS ₂	24
Figure 2.4: How different edge terminations can affect the shape of MoS ₂ domains.	25
Figure 2.5: (Left) MoS ₂ domains produced from non-optimized CVD conditions. (Right) Boat used to hold MoO ₃ for optimized conditions.	25
Figure 2.6: Process developed for transferring MoS ₂	27
Figure 2.7: Typical sample retrieved from mechanical exfoliation process	28

Figure 2.8: (Left) Major Raman modes used in identification of monolayer MoS ₂ . (Right) Graph of frequency difference between major modes versus the layer thickness confirmed using AFM. ¹⁴	29
Figure 2.9: (Top) Monolayer MoS ₂ domains on SiO ₂ /Si wafer. (Bottom) Raman spectra of major modes indicating 1 layer material.	30
Figure 2.10: Graph of photoluminescence for relevant exciton at 680 nm.	31
Figure 2.11: 2D photoluminescence map of MoS ₂ monolayer domains.	32
Figure 2.12: AFM image across a singular monolayer MoS ₂ domain.....	33
Figure 2.13: Optical images of MoS ₂ transferred to a multitude of surfaces for other projects not mentioned in this thesis.	33
Figure 3.1: Illustration of phase transition in MoS ₂ when illuminated in the presence of LiPF ₆ . a) Schematic showing phase transition occurring in LiPF ₆ -PC solution when illuminated. b) Energy band diagram indicating phase transition in the presence of excess electrons. Propylene carbonate's redox potential falls above the 2H valence band.	38
Figure 3.2: Structure of propylene carbonate.....	38
Figure 3.3: Process used to seal MoS ₂ with 1M LiPF ₆ in PC.	40
Figure 3.4: Reciprocal space diagram for 2H MoS ₂ . ¹⁰	41
Figure 3.5: a) Original discovery of MoS ₂ from exfoliated samples. ⁹ b) As exfoliated 1T MoS ₂ . ¹⁷ c) As exfoliated 1T MoS ₂ . ¹⁸ d) 1T MoS ₂ produced from electrons donated from irradiated gold nanoparticles. ²⁴ e) As exfoliated 1T MoS ₂ . ²⁵	41
Figure 3.6: 12X microscope image in XPS.	42

Figure 3.7: Simplified band diagram showing redox position of ACN and PC relative to valence band edge.	44
Figure 3.8: Method for creating simple MoS ₂ based thin film transistors using traditional lithography.	47
Figure 3.9: Process used to create MoS ₂ two terminal devices with nanowire sized spacing.	47
Figure 3.10: Sample under electrochemical testing.	48
Figure 3.11: Raman spectrum showing the partial evolution of 1T phase MoS ₂ under illumination.	49
Figure 3.12: Raman spectra of relevant modes after sample was taken out of solution and washed using methanol.	50
Figure 3.13: a) XPS spectra showing Mo doublet peaks before phase conversion. b) XPS spectra after partial phase change indicating a shift in these peaks to lower binding energies.	51
Figure 3.14: Adventitious carbon peak used as a reference.	52
Figure 3.15: AFM image of monolayer MoS ₂ domain before and after phase change process.	53
Figure 3.16: a) 2D mapping of PL of monolayer domain at start. b) 2D mapping of PL after fifth scan. c) Intensity drop in PL for a monolayer sample. d) Tail end of graph in c showing exponential relationship.	54

Figure 3.17: Full scans of sample in Figure 3.13. There is some drift evident as the sample is scanned.....	55
Figure 3.18: Time at which PL was quenched versus the output power density.	56
Figure 3.19: a) Typical drop in PL seen when using 1M LiPF ₆ in PC. b) PL after 1 hour exposure exposure to just PC. c) PL after 1 hour exposure to 1M LiPF ₆ in ACN. d) PL after 1 hour exposure to a 785 nm laser in 1M LiPF ₆	57
Figure 3.20: (Left) Dry MoS ₂ domains. (Right) MoS ₂ domains after exposure to a 532 nm laser for five seconds.	58
Figure 3.21: PL Before (red) and after (black) being exposed to a 532 nm laser in PC. There is a slight drop in the A exciton and an increase in the B exciton.	58
Figure 3.22: An IV curve of the same device before and after being exposed to a 532 nm laser for one hour in 1M LiPF ₆ solution. The inset at a shows that the before curve was not perfectly flat.	59
Figure 3.23: A Raman spectra of MoS ₂ in between two electrode arms while being exposed to MoS ₂ in 1M LiPF ₆ in PC solution. This graph shows the intensity of the Raman spectra at 1V.	60
Figure 4.1: A comparison of ITO, FTO and Ag NW network bent to 5 mm.	64
Table 4.1: Reported values for individual nanowire junctions from various literature sources. ²³	67
Figure 4.2: Setup used to perform plasmonic nanowelding on silver nanowire mesh.	70
Figure 4.3: Process used to create nanowire mesh based devices	72

Figure 4.4: AgNW mesh on PET under probe station.	72
Figure 4.5: Testing chamber for 80 deg C/100% humidity testing condition.	73
Figure 4.6: Transmission line measurement graph as an example used to calculate contact resistances.	75
Figure 4.7: a) Silver nanowire solution produced in mass. b) Low magnification SEM image showing nanowires are quite long. c) Higher magnification SEM image.	76
Figure 4.8: c) TEM image reveals 6 nm gold coating. d) SEM image of Ag@Au NWs. e,f,g) EDS mapping over a single Ag@Au NW (red is gold, silver is green) h) Line scan showing Au is present across the entire surface.	77
Figure 4.9: SEM images of Ag@Au NWs as compared to Ag NWs after being exposed to atmosphere.	78
Figure 4.10: AgNWs dropcasted on glass substrate.	78
Figure 4.11: SEM image of AgNWs after plasmonic nanowire welding.	79
Figure 4.12: Transparency in the visible range for measured sheet resistances.	80
Figure 4.13: Comparing overall resistance to starting resistance (R/R_0) for nanowire meshes over time for 80 deg C condition.	81
Figure 4.14 Comparing overall resistance to starting resistance (R/R_0) for nanowire meshes over time for 80 deg C condition.	82

Chapter 1

Introduction: Low-dimensional flexible electronics

1.1 The development of flexible electronics

Traditionally, electronic device fabrication including transistors, has been limited to using rigid substrates like silicon.¹ However, current research has been directed toward the development of flexible technology because of the potential for extremely valuable device applications. Devices only thought to exist theoretically such as conformable sensors in health care, electronic readers, smart watches and electronic skin for robotic elements are now closer to becoming a reality.² These electronic devices are advantageous because of their better durability, lighter weight, higher space efficiency and improved comfort.¹

The road to the development of these flexible technologies has been a long one. In 1965, Gordon E. Moore, the cofounder of Intel, made the observation that the number of transistors in a dense digitally integrated circuit doubles essentially every two years largely because of the attractiveness of reduced cost caused by integrating more and more functions on a single chip. This reduction in cost has largely driven the production of smaller and smaller electronic components.³

Besides the reduction in size of electronic components, researchers have also been working on increasing their flexibility. In the 1960s, the first flexible solar cell arrays were made by thinning single crystalline silicon wafers down to about one hundred microns and assembling them in arrays on plastic substrates. Between 1967 and 1979, Peter Brody at the Westinghouse Corporation developed the first reported thin film

transistors (TFTs) on a variety of flexible substrates including mylar, polyethylene and aluminized wrapping foil. Driven by the energy crisis of 1973, researchers at RCA laboratories also reported a Pt/a-Si:H Schottky barrier solar cell made on stainless steel. Then in the early 1980s, these were produced on plastic film substrates and roll to roll fabrication of these devices was introduced. At the same time, Japanese workers in the active-matrix liquid crystal display industry adopted the same plasma enhanced chemical vapor deposition systems used to make a-Si:H solar cells to work on a-Si:H TFTs for liquid crystal displays. This push for flexible liquid crystal displays has continuously caused this technology to further develop.⁴

1.2 Flexible optoelectronic devices made from transition metal dichalcogenides

Traditional silicon based metal-oxide semiconductor field-effect transistors (MOSFETs) form the basic building blocks of all modern electronics that we know of today.⁵ In a typical n-channel transistor design, two n-type semiconductor regions are separated by a p-type semiconducting region typically made of doped silicon. An insulating layer, typically silicon dioxide, sits on top of the middle channel region and is connected to a metal contact known as the gate. In this configuration, when a high enough positive voltage is applied to the gate, it creates a channel between the n-type regions allowing current to flow through the device. When current is flowing, the transistor is said to be in the “on” state as opposed the “off” state when there is not

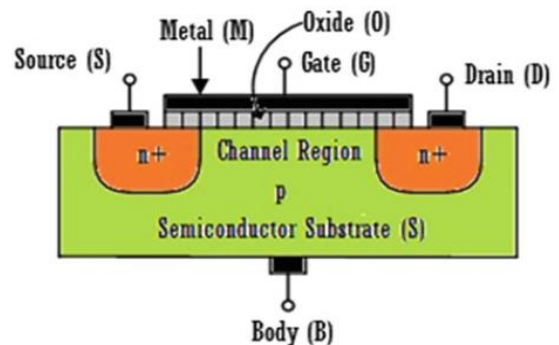


Figure 1.1: A typical MOSFET.⁵

enough positive bias to create a channel. The “on” or “off” states of these transistors allow our electronic devices to make decisions based on input put into a user interface.

However, in an effort to increase operational speed and incorporate more components on a single chip, the channel length between the source and drain regions has continuously been shortened. This has caused what is known as “short channel” effects to occur that leads to a drop in threshold voltage (changing the characteristics of the overall device) and an overall drop in carrier mobility.⁶

Other silicon based architectures have been looked at including FinFETs to get around the inherent limitations of planar transistor technology. However, there are still design complexities associated with these new structures that need to be addressed including scaling issues at low nanometer channel lengths.⁷ With the inherent limitations of silicon based computing such as increasing design complexity, power consumption and heat dissipation, researchers are now looking for new materials that will serve as beneficial alternatives.⁸

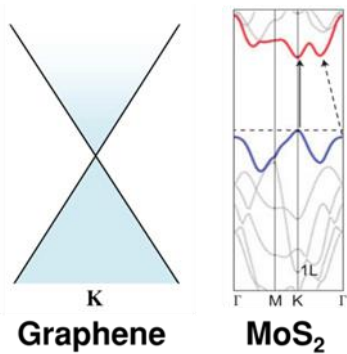


Figure 1.2: (Left) Band structure of graphene. (Right) Band structure of monolayer MoS₂.¹⁰

After the experimental discovery of graphene in 2004, monolayer materials such as graphene and layered transition metal dichalcogenides (TMDs) are being studied intensely for their application in electronic devices.⁹ There is a key difference between graphene and TMDs however, which is the presence of a band gap (see *Figure 1.2*). Graphene is a native semi-metal with conduction and valence bands meeting at the Dirac point, resulting in a zero band gap material.¹⁰ TMDs, such as MoS₂, in contrast have conduction and valence bands

situated at the k point Brillouin zone edge but with different electron energies according to which TMD it is. In the case of MoS₂, this energy difference is 1.8-1.9 eV, making it a direct band gap semiconductor.¹ This presence of band gap essentially means TMDs can be turned on or off making them easier to use in electronic devices rather than graphene which has to have a band gap induced through strain engineering or by confining it to nanoribbons.¹¹ This makes monolayer MoS₂ interesting for creating optoelectronic devices.

TMDs also have relatively good carrier mobility, photo response and outstanding electrostatic gate response making them interesting candidates for optoelectronics and nanoelectronics. Field effect transistors (FET) made using TMDs, in particular MoS₂ and WS₂, have been widely studied due to their excellent electronic properties including high on/off ratios (exceeding 10⁸), immunity to short channel effects, and abrupt subthreshold switching (74 mV/decade).^{12,13,14,15}

MoS₂ is most likely the most important semiconducting material for flexible electronics that require high speed and low power. MoS₂ is naturally immune to the short channel effects suffered by silicon based transistors. It can be functional up to 10,000 cycles of bending up to 1 mm curvature.¹⁶ It has a carrier mobility of 1-400 cm²/V·s, (depending on preparation method and presence of 1T MoS₂)¹⁰ and contains a direct band gap making it usable for optoelectronics.¹ It can readily be produced by chemical vapor deposition strategies on a variety of substrates including glass.¹⁷ It can also be transferred to a variety of substrates if needed.¹⁸ In order to further improve on the device performance, research efforts have been focused on investigating the contact

mechanism, techniques to improve carrier mobility, and study of the limitations in carrier transport.^{19,20,21,22,23,24}

1.2.1 The application of phase change for improving contact resistance in MoS₂ based flexible transistors

With all of the previous advances in flexible thin film transistor technology, one would expect there to be a lot of products on the commercial market. Revenue from flexible electronics is projected to be 300 billion U.S. dollars by 2028.²⁵ However, technological barriers have prevented the commercialization of such technology. These technological barriers are unique to each material and heterostructure. Also, when having to change one material in such a small heterostructure, you likely have to change the rest of the device as well.⁹

One such major problem with using MoS₂ in electronics is the high contact resistance at the MoS₂-metal interface. There is Schottky barrier that exists at this interface preventing high mobility values and resulting in .7-1.0 k Ω per micron sheet resistances.¹² Metal-2H phase TMD contacts create resistances an order of magnitude higher than traditional silicon based devices.²⁶ However, there is the possibility of overcoming this high resistance through the application of using 1T phase MoS₂.

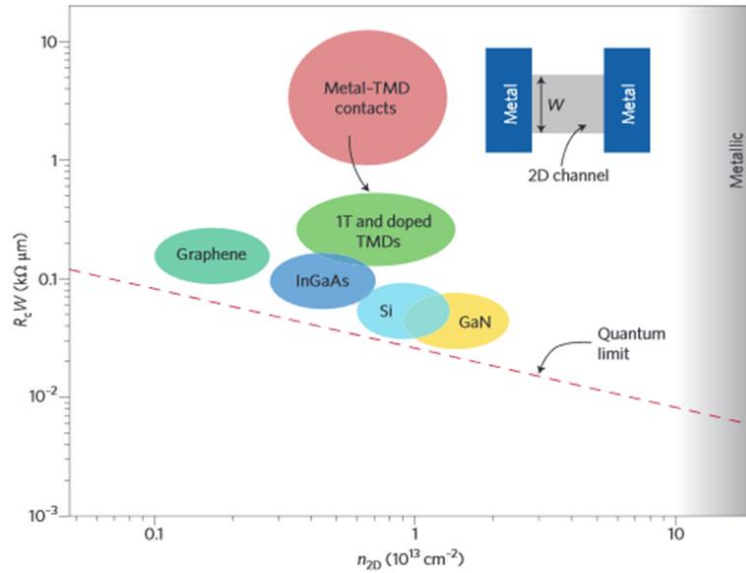


Figure 1.3: Contact resistance dominates resistance in TMD based devices.²⁷

It is well-known that TMDs, including MoS_2 , can have several different phases, such as semiconducting 2H phase (trigonal prismatic D_{3h}) and metallic 1T phase (octahedral O_h).^{8,28,29} Consequently, the two phases have different electronic band structure and other properties

such as carrier mobility and optical absorption efficiency in the visible range.^{30,31,32,33}

This metallic phase has benefits mainly toward hydrogen evolution focused catalysis and the creation of

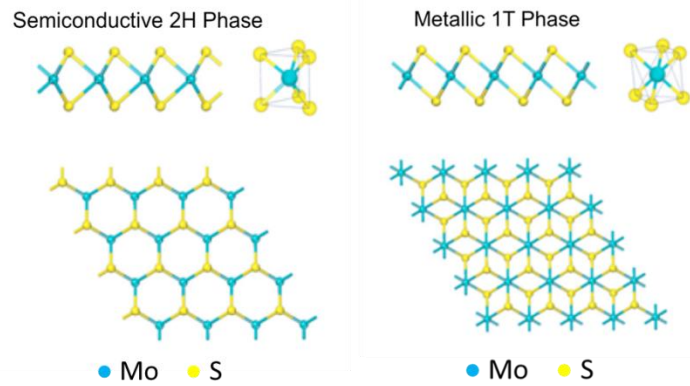


Figure 1.4: Two different phases of MoS_2 , the 1T (Octahedral phase) and 2H (Trigonal prismatic phase).⁶⁰

TMD based electronic components. Typically, hydrogen evolution is done with expensive Pt-based electrocatalysts. However, new TMD based catalysts have the

potential to be low cost and earth abundant.³⁴ Chemically exfoliated 1T MoS₂ monolayer sheets exhibit substantially better reaction kinetics than those in the 2H phase as indicated by an exceptionally low Tafel slope of 40 mV/decade. This is comparable to Pt based catalysts.³⁵

Traditionally, 2H to 1T phase transition is realized through alkali metal (Li⁺, Na⁺ or K⁺) intercalation using highly reductive organometallic compounds and has been studied for about three decades.^{12,36,37,38,39,40} TMDs possessing lamellar structures that can

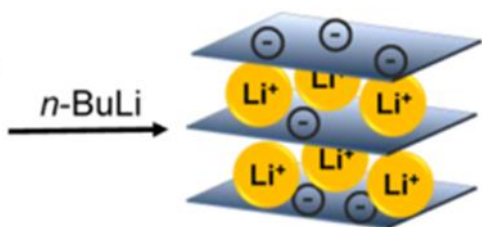


Figure 1.5: Li⁺ ions intercalated between negatively charged MoS₂ layers.⁴¹

serve as hosts for the intercalation of a wide variety of electron-donating chemicals ranging from Lewis bases to alkali metals. One well-known class of intercalatants is the organolithium compounds, which is widely used as a chemical route for preparation of mono- or few layer TMDs.^{41,42,43,44} In these preparations, TMDs are intercalated with lithium to give the reduced Li_xMX_n phase (X=Se, S and so on)an expanded lattice, which can be exfoliated in a second step into monolayer films by an ultrasound-assisted hydration process. Octahedral 1T MoS₂ spontaneously forms under lithium intercalation. This process has been extensively modeled.^{45,46,47}

The mechanism can be understood through a model we have developed based on crystal field theory. As an example, in 2H-MoS₂, the D_{3h} symmetry in the crystal field

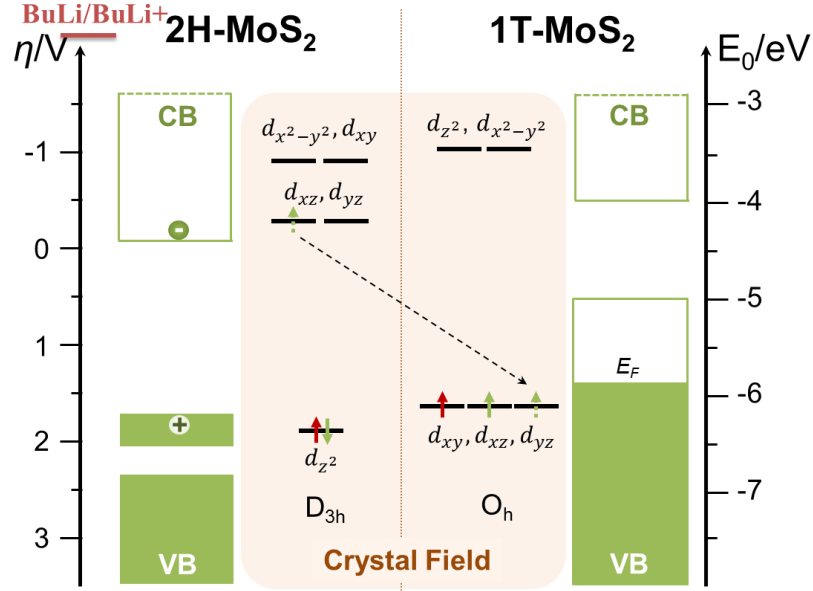


Figure 1.6: Simplified band structure diagram showing change from 2H to 1T MoS₂.

splits Mo 4d orbitals into 3 groups (**Figure 1.6**, left): an a orbital ($4d_{z^2}$), degenerate e' orbitals ($4d_{xz}$ and $4d_{yz}$), and e'' ($4d_{x^2-y^2}$ and $4d_{xy}$) orbitals. $4d_{z^2}$ is the most stable of the three groups. The Mo atom has a d^2 configuration, and both electrons, so both 4d-electrons fill in $4d_{z^2}$, making it completely occupied, while leaving the rest of the higher energy 4d orbitals empty. The complete occupation of the $4d_{z^2}$ orbital, which correspond to the valance band in its electronic band structure, renders 2H semiconducting. On the contrary, the O_h symmetry in 1T-MoS₂ splits the 4d orbitals into 2 groups (**Figure 1.6**, right): the lower energy t_{2g} orbitals ($4d_{xy}$, $4d_{xz}$ and $4d_{yz}$) and the higher energy e_g^* orbitals ($4d_{z^2}$ and $4d_{x^2-y^2}$). The Mo atom has a d^2 configuration, and both electrons fill in 2 of the 3 t_{2g} orbitals at the ground state. The S 3p states do not influence the

electronic structure of the materials, as they are located approximately 3 eV away from the Fermi level. Since the $4d_{z^2}$ orbital in 2H-MoS₂ is slightly more stable than the t_{2g} orbitals in 1T-MoS₂, the total energy of Mo 4d-electrons are also lower, rendering the 2H phase thermodynamically favored. Meanwhile, the incomplete occupation of the 1T t_{2g} orbitals indicates a partially occupied valence band, making the 1T phase metallic.⁴⁸

However, the large crystal field stabilization energy in D_{3h} symmetry makes the e' orbitals in 2H-MoS₂ much higher in energy than $4d_{z^2}$, so when 2H-MoS₂ accepts an extra electron and becomes d³ configuration, that electron is forced into the high energy e' orbitals, destabilizing the 2H phase. This electron can be inserted directly into the conduction band from a highly reducing species such as an organolithium species like n-butyllithium (**Figure 1.6**, left top). These compounds are powerful reductants, with redox energies much higher than the 2H e' states and are capable of direct injection of electrons to this level and reduce MoS₂. The extra negative charge on MoS₂ is balanced and stabilized by Li⁺ absorbed on the MoS₂ sheets to form a transitional Li_xMoS₂ compound. The triply degenerate t_{2g} orbitals in 1T phase are able to accommodate all three 4d electrons in the d³ Mo orbital and reach stable half-filled configuration. Since t_{2g} in 1T-

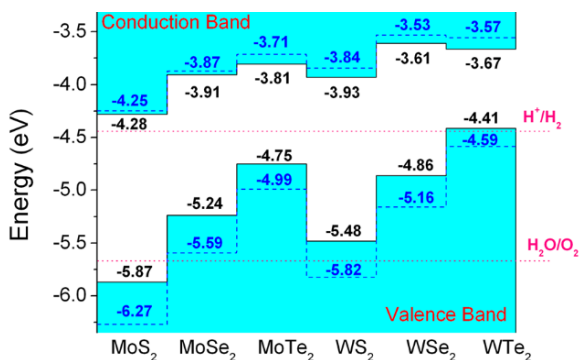


Figure 1.7: Simplified band structures for other TMDs.⁵¹

MoS₂ is much lower in energy than e' orbitals in 2H-MoS₂, the total energy of the d³ configuration is considerably lower in the 1T phase, thus allowing phase conversion to occur.^{49,50}

This methodology has been shown to work across the board for other

relevant TMDs as well. This is because the band structures for other TMDs like MoSe₂ and WS₂, as seen in **Figure 1.7**, have similar energies.⁵¹ The conduction band minimum is well below the redox potential energy of organolithium compounds such as t-butyl lithium at -2.20 V (-2.24 eV vs. vacuum). Phase transformation has been experimentally proven for such transitions as 2H WS₂ to 1T WS₂ and even transition from 1T TaS₂ to 2H TaS₂.^{52,53}

Chhowalla's group has experimentally demonstrated that 1T-phase MoS₂ can significantly decrease the contact resistance to ~200-300 Ω μm at room temperature, (shown to be ~1000 Ω μm in devices using just 2H MoS₂),³³ an impressive level that is getting close to the best contact resistance between graphene and palladium reported by IBM (110±20 Ω μm at 6 K).⁵⁴ Theoretical studies have revealed that the metallic phase of MoS₂ has distinguished electrical properties.⁵⁰ More specifically, it is found that the electron and hole mobility in 1T-MoS₂ are $6.4 \times 10^4 \text{ cm}^2 \text{ V}^{-1} \text{ s}^{-1}$ and $5.7 \times 10^4 \text{ cm}^2 \text{ V}^{-1} \text{ s}^{-1}$, respectively, which are about two orders higher than that in 2H-MoS₂ ($1.2 \times 10^2 \text{ cm}^2 \text{ V}^{-1} \text{ s}^{-1}$ for electrons and $3.8 \times 10^2 \text{ cm}^2 \text{ V}^{-1} \text{ s}^{-1}$ for holes).⁵⁰ This material can be used to improve the performance of TMDs-based nano-electronics and optoelectronics.^{37,55,56,57,58,59}

Besides the spontaneous 2H to 1T phase change in MoS₂ induced by lithium reacting, several methods have been approached to control the phase change including electron bombardment using an *in situ* scanning

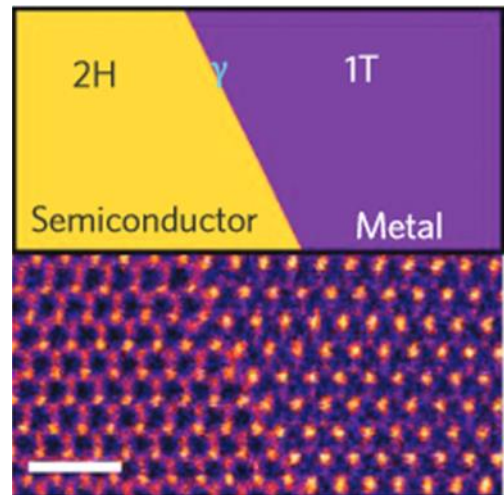


Figure 1.8: Result of Re doped SEM scanning producing 1T MoS₂.⁶⁰

transmission electron microscopy to induce phase change and generate coherent in-plane heterojunction structures,⁶⁰ electron doping from hot electron induction,⁶¹ and pressure induced phase change in bulk TMDs.⁶² However, these processes, due either to the surface modification by Au nanoparticle, slow processing speed of the TEM, or inability of pressure induced change to occur with monolayer films, are not compatible with microelectronic fabrication for further large-scale device development. Thus, there needs to be a different method to convert 2H-MoS₂ to 1T-MoS₂ as discussed in chapter three.

1.3 The need for indium tin oxide alternatives in modern flexible electronics

Indium tin oxide (ITO) is the major conductive electrode in flexible touch screens today and makes up 93% of the market share for conductive materials used in these products. It has been used because it has low sheet resistance at relevant transparencies (>90% for 10 ohms/sq on glass).⁶³ However, indium has a host of undesirable properties that make alternatives more attractive. Most importantly, indium is a ceramic material and is thus brittle and incompatible with flexible substrates, especially those prepared using roll to roll manufacturing.⁶⁴ Even if transferred onto a flexible substrate, ITO cannot stretch as much as flexible substrates which causes micro cracks in the ITO to form thus damaging the film.⁶⁵ It is also currently suffering from what is known as high supply risk, (defined as metals that have small geological resources relative to their current demands and that are mainly recovered as byproducts of other metals). This is because of the huge demand from the worldwide electronics industry.⁶⁶

Current ITO films are also incompatible with flexible substrates because of the elevated temperatures (>350 deg C) needed to grow them through commercial sputtering processes. They are usually grown under an argon-oxygen rich environment as well, thus

making the only possible substrates those that are highly thermal and oxygen resistant.⁶⁷ On top of that, this sputtering process causes up to 70% of the material to be lost on the side walls of the sputtering vessel. Thus, there needs to be an alternative for ITO that has the same level of performance or better.⁶³

There have been several flexible alternatives proposed for indium tin oxide including carbon nanotube meshes, graphene, conductive polymers and organic semiconductors.^{68,69,70} However, each one of these have their drawbacks. Carbon nanotube meshes are limited because of the high contact resistance at individual carbon nanotube junctions.⁷¹ Graphene, though highly conductive, flexible and transparent currently has issues with scaling up the material to be used in mass.⁷² Conductive polymers, though moldable to many different surfaces, do not have the necessary low enough resistance values for use in high current applications. Though, work is being done such as doping to improve the conductivity of these materials.⁷³

Organic semiconductors are a highly competitive alternative as well. They are inherently flexible and can handle strain. In addition, they have the possibility of being incorporated into TFTs through roll to roll printing.^{74,75} However, there are current issues with the lifetime of these materials as they openly react with ambient light, oxygen and water vapor causing degradation. Thus, there is a long time to go before commercialization can occur.⁷⁶ Metal nanowire networks based on silver could be a viable alternative and will be addressed in chapter four of this document.

1.4 Objectives of this work

In this thesis we will be looking at two fundamental problems and how to resolve them:

1. Developing a benign photochemical method for phase change in MoS₂.

2. Corrosion of silver nanowire based networks.

As per discussion formulated above to the need of new types of electronics, there are several objectives to address these issues.

a) **Objective 1:** Develop a scalable route to the formation of monolayer MoS₂ based on chemical vapor deposition that results in large area high quality monolayers. Mechanical exfoliation is explored to develop large area monolayer film. Then, different parameters of chemical vapor deposition are adjusted including pressure, precursor amount, the precursors themselves, and flow rate. A transfer method is developed to transfer MoS₂ to a multitude of surfaces including flexible PDMS. The MoS₂ film is characterized using Raman spectroscopy, photoluminescence and atomic force microscopy (AFM).

b) **Objective 2:** Develop a scalable phase change method that results in the creation of 1T MoS₂ that can be used in flexible TMD devices. First, a mechanism is proposed that is based on the theory of phase change in MoS₂. Then, it is tested using a simple, repeatable structure and analyzed using Raman spectroscopy, photoluminescence, X-ray photoelectron spectroscopy (XPS) and AFM. Control tests are run to validate the proposed mechanism. Simple two terminal devices are created to test the effect of phase change on the device IV curve. Finally, a purely electrochemical method is tested to see if phase change can be induced using current.

c) **Objective 3:** Develop and test electrodes based on gold coated silver nanowires. A method is developed by our lab to coat silver nanowires with a conformal gold coating. This is then developed into a mesh structure and coated onto glass and

flexible PET. The electrical stability of the nanowires is then tested over time and transparencies are measured versus sheet resistance.

1.5 Organization of this thesis

Chapter 2 discusses the routes of creating monolayer MoS₂ first through mechanical exfoliation and then ultimately through chemical vapor deposition under several different conditions. Chapter 3 discusses the invention of a photochemical method for phase change in monolayer MoS₂. Chapter 4 discusses the creation of gold coated nanowire based meshes and their characteristics. Chapter 5 contains the concluding remarks of this dissertation along with suggestions for future work.

1.6 References

1. Kim SJ, Choi K, Lee B, Kim Y, Hong BH. "Materials for flexible, stretchable electronics: graphene and 2d materials." *Annu Rev Mater Res* 2015;45(1):63–84.
2. Harris KD, Elias AL, Chung HJ. "Flexible electronics under strain: a review of mechanical characterization and durability enhancement strategies." *J Mater Sci*. 2016;51(6):2771–805.
3. Moore GE. "Cramming more components onto integrated circuits" *Electronics* 1965;38(8):82–5.
4. Wong, William S., Salleo A. *Flexible Electronics*. 2009.
5. Alsaiif B. *Introduction to Nano*. 2015.
6. Khanna VK. *Integrated Nanoelectronics*. 2016.
7. Shrivastava M, Mehta R, Gupta S, Agrawal N, Baghini MS, Sharma DK, et al. "Toward system on chip (SoC) development using FinFET technology: Challenges, solutions, process co-development & optimization guidelines." *IEEE Trans Electron Devices*. 2011;58(6):1597–607.
8. van der Zande AM, Huang PY, Chenet D a, Berkelbach TC, You Y, Lee G-H, et al. "Grains and grain boundaries in highly crystalline monolayer molybdenum disulphide." *Nat Mater* 2013;12(6):554–61.
9. Geim AK, Grigorieva I V. "Van der Waals heterostructures." *Nature* . 2013;499(7459):419–25.
10. Song I, Park C, Choi HC. "Synthesis and properties of molybdenum disulphide: from bulk to atomic layers." *RSC Adv* . 2015;5(10):7495–514.
11. Chen Y-C, de Oteyza DG, Pedramrazi Z, Chen C, Fischer FR, Crommie MF. "Tuning the bandgap of graphene nanoribbons synthesized from molecular precursors." *ACS Nano* . 2013;(7):6123–8.
12. Mohite AD, Chhowalla M. "Phase-engineered low-resistance contacts for ultrathin MoS₂ transistors." *Nat Mater*. 2014;13
13. Yoon Y, Ganapathi K, Salahuddin S. "How good can monolayer MoS₂ transistors be?" *Nano Lett* . 2011;11(9):3768–73.
14. Song J, Park J, Lee W, Choi T, Jung H, Lee CW, et al. "Conformal synthesis of tungsten disulfide nanosheets using atomic layer deposition." *ACS Nano*. 2013;7:11333–40.

15. Liu E, Fu Y, Wang Y, Feng Y, Liu H, Wan X, et al. "Integrated digital inverters based on two-dimensional anisotropic ReS₂ field-effect transistors." *Nat Commun* . 2015;6(May):6991.
16. Chang HY, Yogeesh MN, Ghosh R, Rai A, Sanne A, Yang S, et al. "Large-area monolayer mos₂ for flexible low-power rf nanoelectronics in the ghz regime." *Adv Mater*. 2016;28(9):1818–23.
17. Li X, Zhu H. "Two-dimensional mos₂: properties, preparation, and applications." *J Mater* . 2015;1(1):33–44.
18. Li H, Wu J, Huang X, Yin Z, Liu J, Zhang H. "A universal, rapid method for clean transfer of nanostructures onto various substrates." *ACS Nano*. 2014;8(7):6563–70.
19. Gong C, Huang C, Miller J, Cheng L, Hao Y, Cobden D, et al. "Metal contacts on physical vapor deposited monolayer mos₂." *ACS Nano* . 2013;7(12):11350–7.
20. Renteria J, Samnakay R, Rumyantsev SL, Goli P, Shur MS. "Low-frequency 1 / f noise in mos₂ transistors." *Nano Lett*. 2013;2:1–18.
21. Radisavljevic B, Radenovic A, Brivio J, Giacometti V, Kis A. "Single-layer MoS₂ transistors." *Nat Nanotechnol* . 2011;6(3):147–50.
22. Kim S, Konar A, Hwang W-S, Lee JH, Lee J, Yang J, et al. "High-mobility and low-power thin-film transistors based on multilayer MoS₂ crystals." *Nat Commun* . 2012;3:1011.
23. Das S, Robinson JA, Dubey M, Terrones H, Terrones M. "Beyond Graphene: Progress in Novel Two-Dimensional Materials and van der Waals Solids." *Annu Rev Mater Res* . 2015;45(1):1–27.
24. Radisavljevic B, Kis A. "Mobility engineering and a metal–insulator transition in monolayer MoS₂." *Nat Mater* . 2013;12(9):815–20.
25. Hu J. "Overview of flexible electronics from ITRI's viewpoint." 2010 28th VLSI Test Symp. 2010;84.
26. Dong L, Lin S, Yang L, Zhang J, Yang C, Yang D, et al. "Spontaneous exfoliation and tailoring of MoS₂ in mixed solvents." *Chem Commun* . 2014;50(100):15936–9.
27. Jena D, Banerjee K, Xing GH. "2D crystal semiconductors: Intimate contacts." *Nat Mater* . 2014;13(12):1076–8.
28. Zhou W, Zou X, Najmaei S, Liu Z, Shi Y, Kong J, et al. "Intrinsic structural

- defects in monolayer molybdenum disulfide." *Nano Lett.* 2013;
29. Tang Q, Jiang D. "Stabilization and band-gap tuning of the 1t-mos₂ monolayer by covalent functionalization." *Chem Mater* . 2015
 30. Guo Y, Sun D, Ouyang B, Raja A, Song J, Heinz TF, et al. "Probing the dynamics of the metallic-to-semiconducting structural phase transformation in mos₂ crystals." *Nano Lett* . 2015;15(8):5081–8.
 31. Xiong F, Wang H, Liu X, Sun J, Brongersma M, Pop E, et al. "Li intercalation in mos₂: in situ observation of its dynamics and tuning optical and electrical properties." *Nano Lett.* 2015;15(10):6777–84.
 32. Voiry D, Yamaguchi H, Li J, Silva R, Alves DCB, Fujita T, et al. "Enhanced catalytic activity in strained chemically exfoliated ws₂ nanosheets for hydrogen evolution." *Nat Mater* . 2013;12(9):850–5.
 33. Acerce M, Voiry D, Chhowalla M. "Metallic 1T phase MoS₂ nanosheets as supercapacitor electrode materials." *Nat Nanotechnol* . 2015;10(4):313–8.
 34. Li Y, Wang L, Zhang S, Dong X, Song Y, Cai T, et al. "Cracked monolayer 1T MoS₂ with abundant active sites for enhanced electrocatalytic hydrogen evolution." *Catal Sci Technol* . 2017;7(3):718–24.
 35. Voiry D, Salehi M, Silva R, Fujita T, Chen M, Asefa T, et al. "Conducting MoS₂ nanosheets as catalysts for hydrogen evolution reaction." *Nano Lett* . 2013;13(12):6222–7.
 36. Park JC, Yun SJ, Kim H, Park JH, Chae SH, An SJ, et al. "Phase-engineered synthesis of centimeter-scale 1t'- and 2h-molybdenum ditelluride thin films." *ACS Nano*. 2015;9(6):6548–54.
 37. Mahjouri-Samani M, Lin M-W, Wang K, Lupini AR, Lee J, Basile L, et al. "Patterned arrays of lateral heterojunctions within monolayer two-dimensional semiconductors." *Nat Commun* . 2015;6:7749.
 38. Py M a., Haering RR. "Structural destabilization induced by lithium intercalation in MoS₂ and related compounds." *Can J Phys* . 1983;61(8):76–84.
 39. Zheng J, Zhang H, Dong S, Liu Y, Tai Nai C, Suk Shin H, et al. "High yield exfoliation of two-dimensional chalcogenides using sodium naphthalenide." *Nat Commun* . 2014;5:1–7.
 40. Tan C, Zhang H. "Wet-chemical synthesis and applications of non-layer structured two-dimensional nanomaterials." *Nat Commun* . 2015;6:7873.

41. Knirsch KC, Berner NC, Nerl HC, Cucinotta CS, Gholamvand Z, McEvoy N, et al. "Basal-plane functionalization of chemically exfoliated molybdenum disulfide by diazonium salts." *ACS Nano* . 2015;9(6):6018–30.
42. Eda G, Yamaguchi H, Voiry D, Fujita T, Chen M, Chhowalla M. "Photoluminescence from chemically exfoliated MoS₂." *Nano Lett*. 2011;11(12):5111–6.
43. Zeng Z, Yin Z, Huang X, Li H, He Q, Lu G, et al. "Single-layer semiconducting nanosheets: High-yield preparation and device fabrication." *Angew Chemie - Int Ed*. 2011;50(47):11093–7.
44. Eng AYS, Ambrosi A, Sofer Z, Šimek P, Pumera M. "Electrochemistry of transition metal dichalcogenides: Strong dependence on the metal-to-chalcogen composition and exfoliation method." *ACS Nano*. 2014;8(12):12185–98.
45. Duerloo K-AN, Li Y, Reed EJ. "Structural phase transitions in two-dimensional Mo- and W-dichalcogenide monolayers." *Nat Commun* . 2014;5(May):1–9.
46. Chen XB, Chen ZL, Li J. "Critical electronic structures controlling phase transitions induced by lithium ion intercalation in molybdenum disulphide." *Chinese Sci Bull*. 2013;58(14):1632–41.
47. Wang L, Xu Z, Wang W, Bai X. "Atomic mechanism of dynamic electrochemical lithiation processes of MoS₂ nanosheets." *J Am Chem Soc*. 2014;136(18):6693–7.
48. Chhowalla M, Voiry D, Yang J, Shin HS, Loh KP. "Phase-engineered transition-metal dichalcogenides for energy and electronics." *MRS Bull* . 2015;40(7):585–91.
49. Cheng Y, Nie A, Zhang Q, Gan LY, Shahbazian-Yassar R, Schwingenschlogl U. "Origin of the phase transition in lithiated molybdenum disulfide." *ACS Nano*. 2014;8(11):11447–53.
50. Kan M, Wang JY, Li XW, Zhang SH, Li YW, Kawazoe Y, et al. "Structures and phase transition of a mos₂ monolayer." *J Phys Chem C* . 2014;118(3):1515–22.
51. Kang J, Tongay S, Zhou J, Li J, Wu J. "Band offsets and heterostructures of two-dimensional semiconductors." *Appl Phys Lett*. 2013;102(1):22–5.
52. Enyashin AN, Yadgarov L, Houben L, Popov I, Weidenbach M, Tenne R, et al. "New route for stabilization of 1T-WS₂ and MoS₂ phases." *J Phys Chem C*. 2011;115:24586–91.
53. Chhowalla M, Shin HS, Eda G, Li L-J, Loh KP, Zhang H. "The chemistry of two-dimensional layered transition metal dichalcogenide nanosheets." *Nat Chem* .

2013;5(4):263–75.

54. Xia F, Perebeinos V, Lin Y, Wu Y, Avouris P. "The origins and limits of metal–graphene junction resistance." *Nat Nanotechnol* . 2011;6(3):179–84.
55. Duan X, Wang C, Shaw JC, Cheng R, Chen Y, Li H, et al. "Lateral epitaxial growth of two-dimensional layered semiconductor heterojunctions." *Nat Nanotechnol* . 2014;9(12):1024–30.
56. Zeng Q, Wang H, Fu W, Gong Y, Zhou W, Ajayan PM, et al. "Band engineering for novel two-dimensional atomic layers." *Mater Views*. 2015;11(16):1868–84.
57. Duesberg GS. "Heterojunctions in 2D semiconductors: A perfect match." *Nat Mater* . 2014;13(12):1075–6.
58. Huang C, Wu S, Sanchez AM, Peters JJP, Beanland R, Ross JS, et al. "Lateral heterojunctions within monolayer MoSe₂–WSe₂ semiconductors." *Nat Mater* . 2014;13(12):1096–101.
59. Gong Y, Lin J, Wang X, Shi G, Lei S, Lin Z, et al. "Vertical and in-plane heterostructures from WS₂/MoS₂ monolayers." *Nat Mater* . 2014;13(12):1135–42.
60. Lin Y-C, Dumcenco DO, Huang Y-S, Suenaga K. "Atomic mechanism of the semiconducting-to-metallic phase transition in single-layered MoS₂." *Nat Nanotechnol* . 2014;9(5):391–6.
61. Kang Y, Najmaei S, Liu Z, Bao Y, Wang Y, Zhu X, et al. "Plasmonic hot electron induced structural phase transition in a mos₂ monolayer." *Adv Mater*. 2014;26(37):6467–71.
62. Nayak AP, Bhattacharyya S, Zhu J, Liu J, Wu X, Pandey T, et al. "Pressure-induced semiconducting to metallic transition in multilayered molybdenum disulphide." *Nat Commun* . 2014;5(May):3731.
63. Ye S, Rathmell AR, Chen Z, Stewart IE, Wiley BJ. "Metal nanowire networks : the next generation of transparent conductors." *Adv Mater*. 2014;6670–87.
64. Renouf C. "A touch of indium." *Nat Chem* . 2012;4(10):862–862.
65. Hamasha MM, Dhakal T, Alzoubi K, Albahri S, Qasaimeh A, Lu S, et al. "Stability of ITO thin film on flexible substrate under thermal aging and thermal cycling conditions." *IEEE/OSA J Disp Technol*. 2012;8(7):383–8.
66. Graedel TE, Harper EM, Nassar NT, Nuss P, Reck BK. "Criticality of metals and metalloids." *Proc Natl Acad Sci* . 2015;112(14):4257–62.

67. Kudryashov D, Gudovskikh A, Zelentsov K. "Low temperature growth of ITO transparent conductive oxide layers in oxygen-free environment by RF magnetron sputtering." *J Phys Conf Ser* . 2013;461:12021.
68. Editor E, Langley D, Celle C, Bellet D, Simonato J. "Flexible transparent conductive materials based on silver nanowire networks: a review." *Nat Nano*. 2013;24.
69. Cai L, Wang C. "Carbon nanotube flexible and stretchable electronics." *Nanoscale Res Lett* . 2015;10(1):320.
70. Shown I, Ganguly A, Chen L-C, Chen K-H. "Conducting polymer-based flexible supercapacitor." *Energy Sci Eng* . 2015;3(1):2–26.
71. Zaumseil J. "Single-walled carbon nanotube networks for flexible and printed electronics." *Semicond Sci Technol* . 2015;30(7):74001.
72. Salavagione HJ. "Covalent graphene-polymer nanocomposites." 2015.
73. Kawakita J, Chikyow T. "Conductive polymer/metal composite for flexible interconnect." *J Appl Phys*.
74. Mei J, Diao Y, Appleton AL, Fang L, Bao Z. "Integrated materials design of organic semiconductors for field-effect transistors." *JACS*. 2013;
75. Root SE, Savagatrup S, Printz AD, Rodriguez D, Lipomi DJ. "Mechanical properties of organic semiconductors for stretchable, highly flexible, and mechanically robust electronics." *Chem Rev* . 2017
76. Yu D, Yang YQ, Chen Z, Tao Y, Liu YF. "Recent progress on thin-film encapsulation technologies for organic electronic devices." *Opt Commun* . 2016;362:43–9.

Chapter 2

Chemical vapor deposition synthesis of high quality monolayer MoS₂

2.1 Introduction

There have been several ways developed to synthesize monolayer MoS₂ over the past few decades. These can be divided into two categories: top down and bottom up approaches.¹ Top down approaches rely on the use of naturally occurring bulk MoS₂ to extract monolayers. Most simply, there is the technique of mechanical exfoliation using Scotch tape to separate several layer flakes from a bulk crystal and then through several iterations of repeated separations, the monolayer MoS₂ is extracted through shear force. There are also methods of chemical exfoliation using such species as butyllithium (BuLi) to cleave layers by allowing ions to intercalate between layers and separate them.²

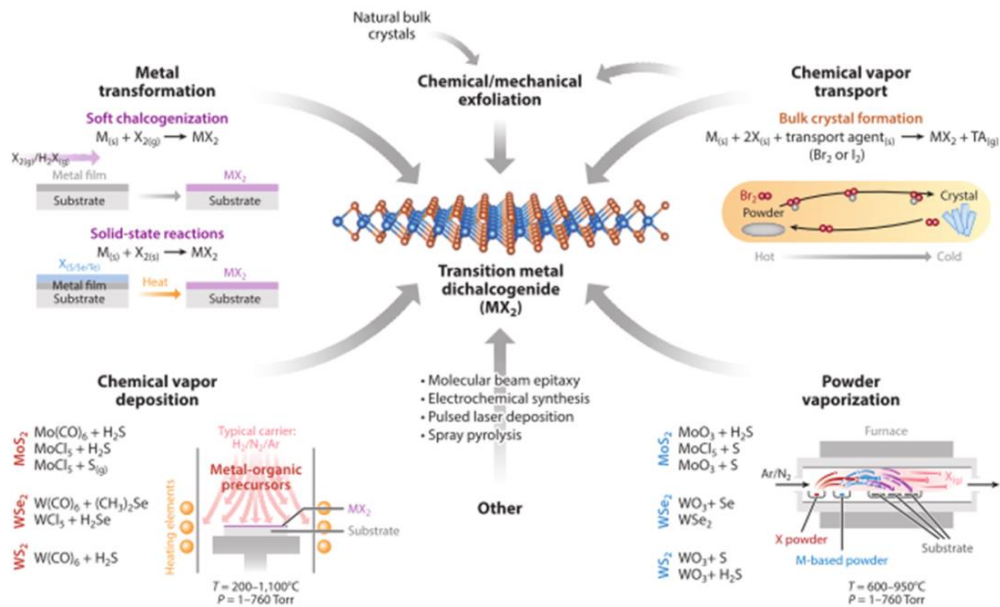


Figure 2.1: The many routes of TMD synthesis.²

Bottom up approaches include those where MoS_2 is formed from chemical precursors, mostly through a form of chemical vapor deposition. MoS_2 can be formed from the thermal decomposition of $(\text{NH}_4)_2\text{MoS}_4$. This involves using $(\text{NH}_4)_2\text{MoS}_4$ as a powder and performing simple thermolysis on a substrate. There is also direct heating of MoS_2 bulk powder which then relies on random nucleation of MoS_2 onto a substrate.⁵

Chemical vapor deposition is a very popular method however, because it is believed to be scalable and low cost.³ Chemical vapor deposition relies on the heating of solid precursors which then mix in the vapor phase to then deposit on a solid substrate that is commonly either silica, silicone or mica.⁵ Specifically, for MoS_2 , much work has been done in an effort to synthesize large area monolayers including the use of solid precursors such as sulfur powder, MoCl_5 and MoO_3 .^{6,4} Work has also been done to produce wafer scale monolayer MoS_2 using gaseous H_2S and solid MoO_3 precursors.⁵

2.2 Experimental details

The first and most obvious method for high quality MoS_2 is the use of mechanical exfoliation as it has been shown in literature to produce high quality MoS_2 samples.⁶ A piece of Scotch tape was pressed onto flake of bulk MoS_2 by hand. The scotch tape was then peeled off and stuck to itself between five and thirty times before being pressed onto a SiO_2 wafer. The SiO_2 surface had been sonicated in acetone and ethanol for twenty minutes each before MoS_2 was deposited. Mechanical exfoliation from bulk material was done but the film created was always variable in terms of the number of layers produced and usually connected to bulk material.

Considering that we would like to look at the properties of only monolayer MoS_2 , we decided to move onto use of chemical vapor deposition to create our MoS_2 films. For

use in CVD experiments, MoS₂ wafers were first sonicated in acetone and ethanol for a period of 20 minutes each. Wafers were then deposited into a piranha (three parts sulfuric acid:one part hydrogen peroxide) solution and let sit at 100 deg C for a period of more than two hours before use. Wafers were extracted from the mixture and washed six time with nanopure water before being finally dried with a nitrogen gun. This method is similar to other literature for the growth of large area MoS₂.⁷ This method was found to be very important in the creation of large area monolayer material.

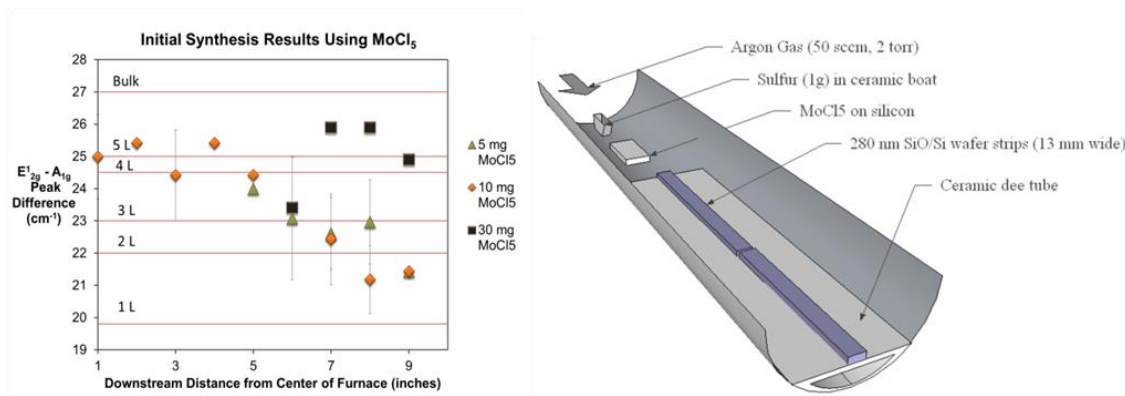


Figure 2.2: (Left) Initial synthesis results using MoCl₅ as a precursor. (Right) 3D model of inside CVD tube for system including conditions for synthesis.

We first tried using a small Lindberg blue furnace with a two inch diameter tube copying a method used by Yu Y. et. al.⁸ This system was brought down to two torr of pressure, with fifty sccm Argon, and used ten minutes at 850 deg C with 30 minutes of ramp time. Differing amounts of MoCl₅ were tried over a series of repeated runs on large area SiO₂/Si wafers at varying distances. A ceramic dee tube was used to pull the substrate in and out with ease. Results proved to be sporadic. We could not achieve a continuous layer of monolayer MoS₂ for our system.

However, it was found that most literature on synthesis of MoS₂ used solid MoO₃ as a precursor.⁹ Thus, it was thought that we should move on to the use of MoO₃ as a precursor as the literature showed we could produce large MoS₂ domains.¹⁰ A large MoS₂ domain would be beneficial toward the resting of electrical devices as typical photolithography cannot pattern correctly below about a ten micron resolution.

We eventually settled on an ambient pressure system for the growth of monolayer MoS₂. The system used twenty sccm argon flowing over .1 grams of solid sulfur powder and sixteen milligrams of MoO₃. The furnace was ramped to 800 deg C at for a total ramping time of 30 minutes. The sulfur powder was heated separately to 130 deg C at the start of the reaction. The tube was a one inch diameter tube made of quartz. The MoO₃ powder was placed at the middle of the furnace where as the sulfur powder was placed nine inches upstream of the furnace center. A diagram can be seen below.

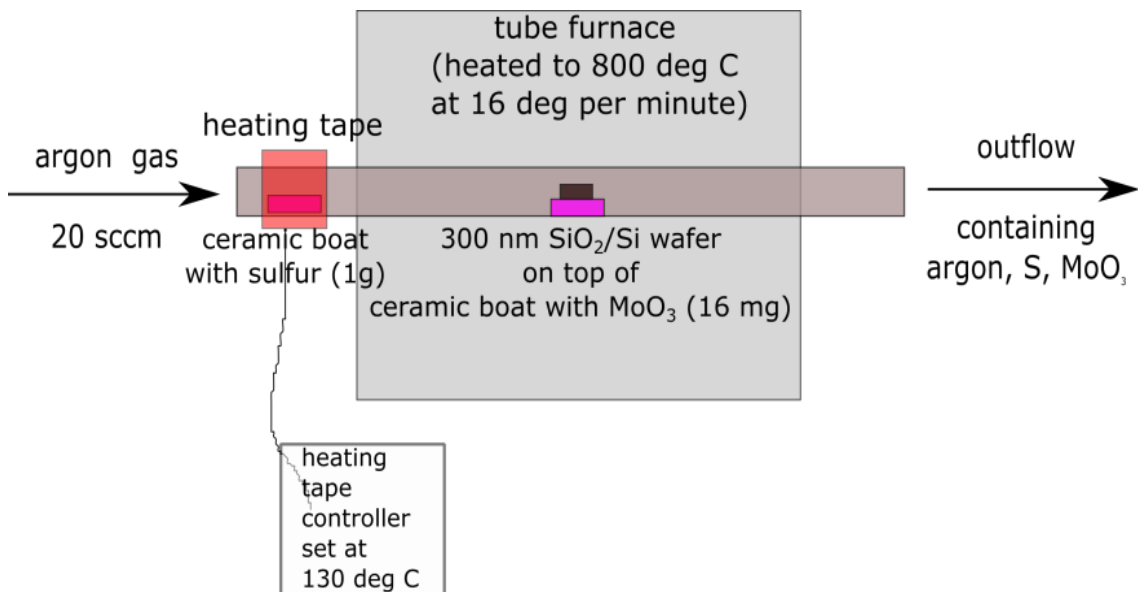


Figure 2.3: Final successful CVD conditions for growth of large area MoS₂.

The boat created for the MoO_3 powder was invented by myself. It was found through previous runs using a different flat ceramic boat that MoS_2 domains ended up being either sulfur or molybdenum deficient. The shape of the individual MoS_2 domains predict whether it has either sulfur or molybdenum terminated edges. Perfect equilateral triangles of MoS_2 are sulfur terminated at all edges. However, if there are other shapes that appear such as octagons or hexagons or even other irregular shapes, then it means that there will be some molybdenum terminated edges on the sample itself.¹¹ This is not believed to affect the quality of the MoS_2 , but is important to keep the sample consistency the same.

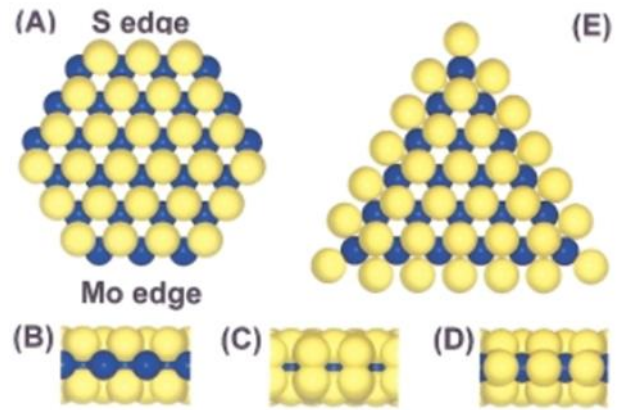


Figure 2.4: How different edge terminations can affect the shape of MoS_2 domains.

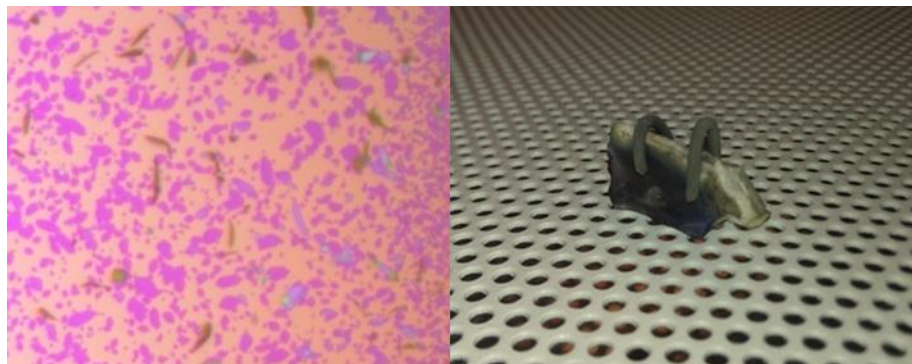


Figure 2.5: (Left) MoS_2 domains produced from non-optimized CVD conditions. (Right) Boat used to hold MoO_3 for optimized conditions.

MoS_2 domains were analyzed using Raman spectroscopy, photoluminescence, and atomic force microscopy to confirm that they were in fact one layer and of high

quality. A Horiba LabRAM spectrophotometer was used for both Raman and photoluminescence readings. For the Raman data, an accumulation time of fifteen seconds was averaged over three readings with a 1800/mm grating. The photoluminescence readings used a seven second accumulation time over three readings with a 600/mm grating. A 532 nm laser was used at a $137 \mu\text{W}/\mu\text{m}^2$ power density. Power output was measured at the point of contact with the sample using a Thorlabs Dual Channel Optical Power and Energy Meter. AFM was done using a AIST-NT SmartSPM 1000 with a AC160TS-R3 Tip from Asylum Research in tapping mode.

In addition, a XYZ piezo stage was interfaced with using LabView and MATLAB to do photoluminescence mapping of our produced domains. This was done to understand photoluminescence across an individual domain. Two dimensional mapping was done at 1s accumulation per pixel using a custom LabView program.

As the growth temperature of TMD monolayers is relatively high, temperature-sensitive substrates (such as polymer-based substrates) cannot be used in the synthetic process, while their use is essential for flexible electronics.⁴ Thus, there needs to be a way to transfer this material from a rigid substrate like silicon dioxide to a flexible one or surfaces like gold under 100 microns that sits on the surface of a flexible substrate. If the MoS_2 domains cannot be transferred onto another flexible substrate, then they essentially are useless for flexible electronics.

This was achieved by using a water based method.¹² Water acts as an agent which disrupts the weak Van Der Waals forces between the MoS_2 monolayer and the SiO_2 . PDMS approximately one millimeter thick was created on a glass slide. Then the bottom surface originally in contact with glass was pressed onto a silica wafer where

monolayer MoS₂ domains had been grown. A corner of the PDMS was then lifted up and droplet of water was placed in between the PDMS and silica wafer. The PDMS was then slowly peeled off and placed on another substrate (gold, silver, glass etc.). A beaker filled with 500 ml of water was then placed on top as a weight and this was heated at 80 deg C for 24 hrs. The PDMS was then peeled off and domains had been transferred to the substrate.

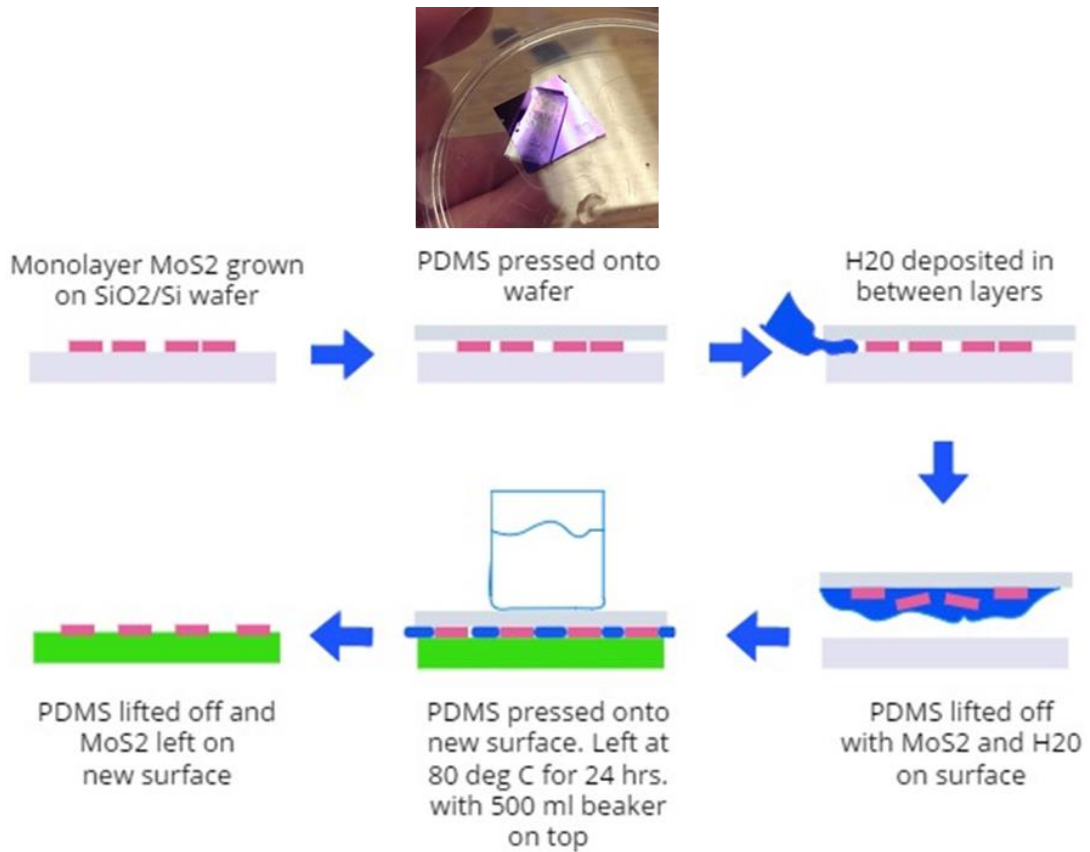


Figure 2.6: Process developed for transferring MoS₂.

2.3 Results and Discussion

2.3.1 Mechanically exfoliated MoS₂

This method produced several mixed layers that were interconnected. On the off chance that we would obtain monolayer MoS₂, it was always attached to multilayer regions, making it unusable for electronic devices or further experiments.

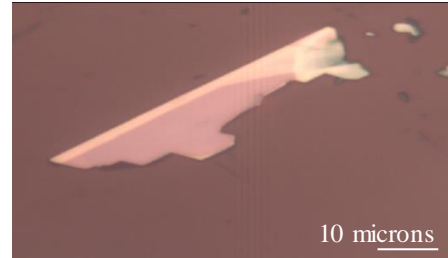


Figure 2.7: Typical sample retrieved from mechanical exfoliation process.

Raman spectroscopy point readings on the MoS₂ layers revealed a mix of layers ranging from two to bulk MoS₂ layers as explained in the next section. This was also quickly identified using the optical images themselves as a rough indicator of layer number.¹³ Optical contrast can indicate differences in layer numbers present.

2.3.2 Raman Spectroscopy of CVD produced MoS₂

Raman results showed that there was monolayer MoS₂ present as a result of the CVD produced system. We got mixed results as a result of boat placement but eventually clearly identified monolayer MoS₂. Some of our MoS₂ ended up being two layers or more. It was clearly identified using the distance between the two major modes E_{2g}¹ and A_{1g}. MoS₂ has 18 phonon modes (3 acoustic and 3 optical modes). The E_{2g}¹ mode represents an in plane vibrational Raman active mode. The A_{1g} represents the an out of plane vibrational Raman active mode. It was found that the distance between these two modes can accurately determine the layer number of MoS₂ samples.¹⁴

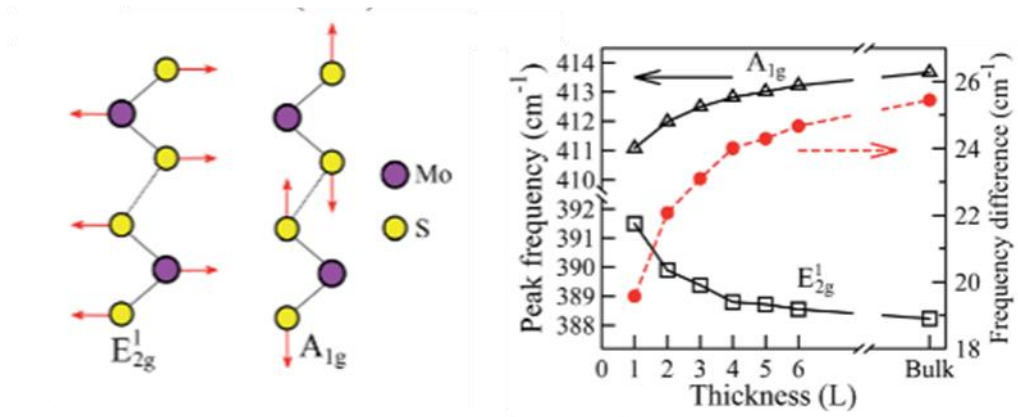


Figure 2.8: (Left) Major Raman modes used in identification of monolayer MoS₂. (Right) Graph of frequency difference between major modes versus the layer thickness confirmed using AFM.¹⁴

This was an easy characterization tool to use as it allowed for rapid identification that is based on the distance between these two active major Raman modes. Interestingly, a one layer sample has a distance of about 19-20 cm⁻¹ between the two modes. From there, the E_{2g}^1 mode red shifts while the A_{1g} mode begins to blue shift as the layer number gets higher.¹⁴ We found that our domains were at 20.1 cm⁻¹ difference between the two Raman modes indicating they were in fact one layer.

Domains usually ended up being about twenty microns long on each side with a triangular shape. Domains grew along the diagonal edges of our samples with the lowest layer (monolayer) samples being closest toward the center.

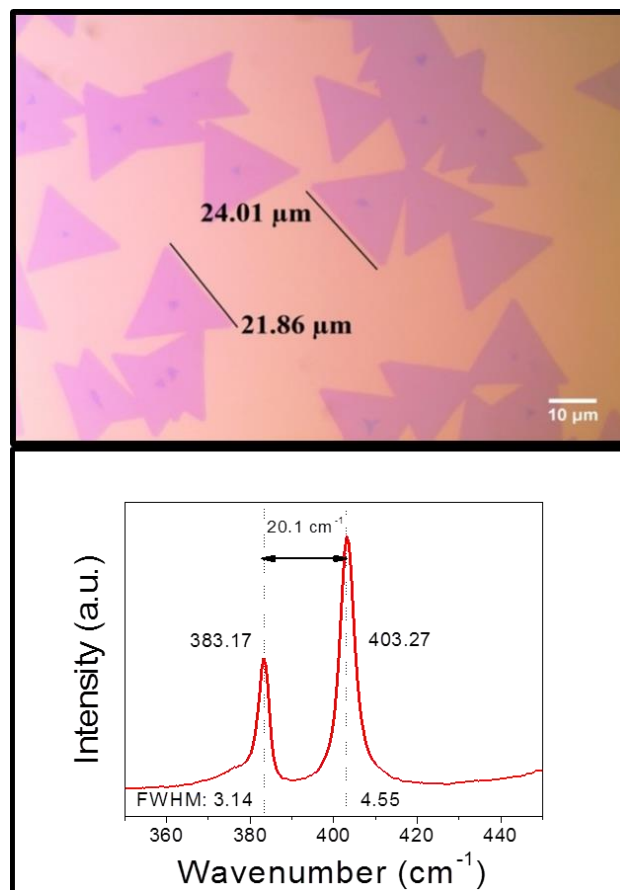


Figure 2.9: (Top) Monolayer MoS₂ domains on SiO₂/Si wafer. (Bottom) Raman spectra of major modes indicating 1 layer material.

2.3.2 Photoluminescence

Photoluminescence is essentially the process of releasing a photon as an electron relaxes back down to the valence band from the conduction band after being initially excited by an external light source with sufficient energy (i.e. laser) to overcome the band gap inherent to the material. The band structure for 2H-MoS₂ reveals that the band gap is a direct band gap in the visible range with a value of about 1.8-1.9 eV.¹⁵ Photoluminescence from the MoS₂ was very strong with a small FWHM of 24.05. This

indicated that the MoS₂ was of high quality and be good for use in optoelectronic devices. It is comparable to other values found in literature.¹⁶

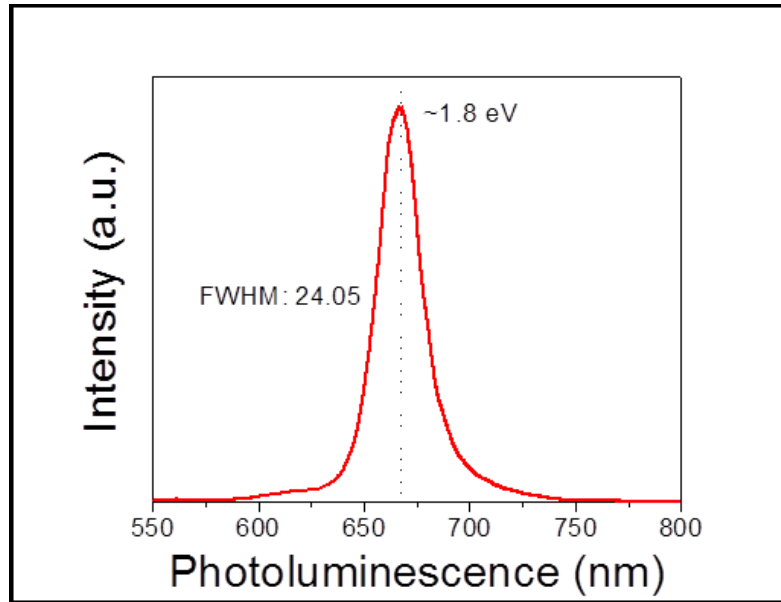


Figure 2.10: Graph of photoluminescence for relevant exciton at 680 nm.

Photoluminescence mapping revealed that domains had a variation in response across each individual domain with the strongest response being at the edges of each domain. This has been shown to occur in multiple literature sources that do mapping of monolayer MoS₂ domains.

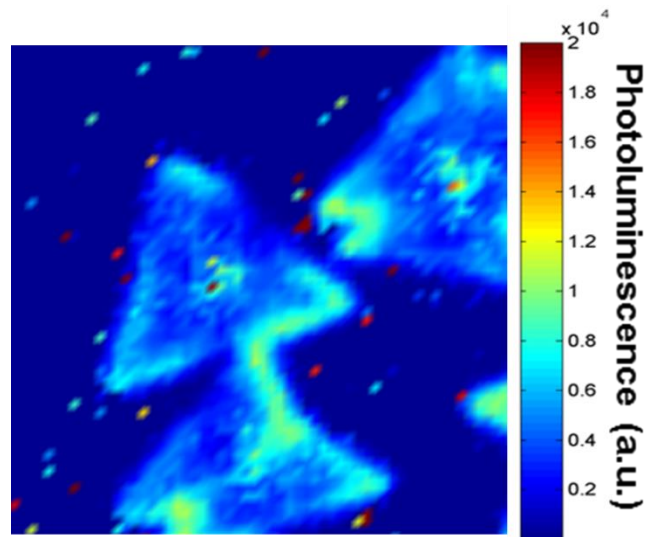


Figure 2.11: 2D photoluminescence map of MoS₂ monolayer domains.

2.3.3 Atomic force microscopy

Our AFM data showed that domains were of little structural defect. There was uniform growth across the domain for final sample runs. The height of MoS₂ domains is reported to be between .65-.9 nm.^{17,18,19} Our data showed that these domains were in fact one layer in height at .7 nm. What we believe to be sulfur particles were also present all over the sample surface itself making the silica surface outside the domain quite rough.

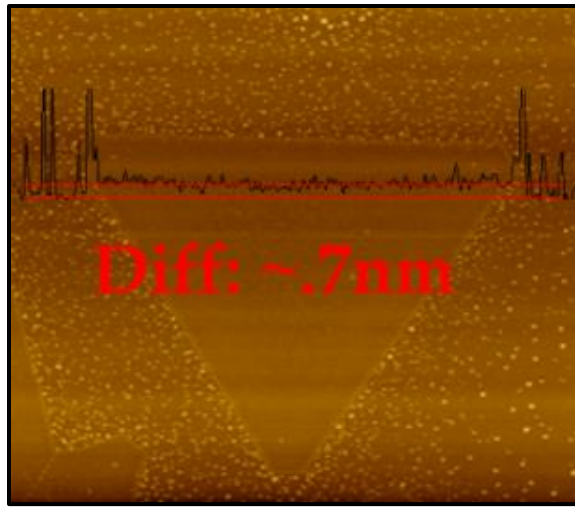


Figure 2.12: AFM image across a singular monolayer MoS₂ domain

2.3.4 Transfer of MoS₂ to other surfaces

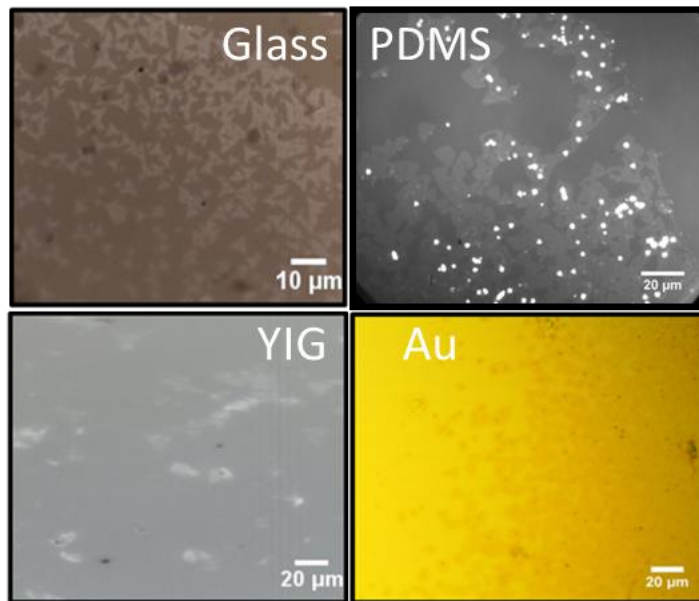


Figure 2.13: Optical images of MoS₂ transferred to a multitude of surfaces for other projects not mentioned in this thesis.

We wanted to show that we could develop a method for transferring to a multitude of surfaces for future projects. MoS₂ could be transferred using this method to

flexible PDMS. It could also be transferred to glass, YIG and gold surfaces as well with the triangular shape of the domains still intact. This method serves as an all-purpose transfer method for our domains.

2.4 References

1. Li X, Zhu H. "Two-dimensional MoS₂: Properties, preparation, and applications." *J Mater.* 2015;1(1):33–44.
2. Das S, Robinson JA, Dubey M, Terrones H, Terrones M. "Beyond graphene: progress in novel two-dimensional materials and van der waals solids." *Annu Rev Mater Res.* 2015;45(1):1–27.
3. Zhang J, Yu H, Chen W, Tian X, Liu D, Cheng M, et al. "Scalable growth of high-quality polycrystalline mos 2 monolayers on sio 2 with tunable grain sizes." *ACS Nano.* 2014;8(6):6024–30.
4. Wang ZM. *MoS₂: Material, Physics and Devices.* 2014.
5. Kim Y, Bark H, Ryu GH, Lee Z, Lee C. "Wafer-scale monolayer MoS₂ grown by chemical vapor deposition using a reaction of MoO₃ and H₂S." *J Phys Condens Matter* 2016;28(18):184002.
6. Li H, Wu J, Yin Z, Zhang H. "Preparation and applications of mechanically exfoliated single-layer and multilayer MoS₂ and WSe₂ nanosheets." *Acc Chem Res.* 2014;47(4):1067–75.
7. Dumcenco D, Ovchinnikov D, Marinov K, Lopez-Sanchez O, Krasnozhan D, Chen M-W, et al. "Large-area epitaxial monolayer MoS₂." 2014;(4):4611–20.
8. Yu Y, Li C, Liu Y, Su L, Zhang Y, Cao L. "Controlled scalable synthesis of uniform, high-quality monolayer and few-layer MoS₂ films." *Sci Rep*
9. Li X, Zhu H. "Two-dimensional MoS₂: Properties, preparation, and applications." *J Mater.* 2015;1(1):33–44.
10. van der Zande AM, Huang PY, Chenet D a, Berkelbach TC, You Y, Lee G-H, et al. "Grains and grain boundaries in highly crystalline monolayer molybdenum disulphide." *Nat Mater.* 2013;12(6):554–61.
11. Helveg S, Lauritsen J V., Laegsgaard E, Stensgaard I, Norskov JK, Clausen BS, et al. "Atomic-scale structure of single-layer MoS₂ nanoclusters." *Phys Rev Lett.* 2000;84(5):951–4.
12. Lee Y, Yu L, Wang H, Fang W, Ling X, Shi Y, et al. "Synthesis and transfer of single-layer transition metal disulfides on diverse surfaces." *Nano Lett.* 2013;
13. Li H, Wu J, Huang X, Lu G, Yang J, Lu X, et al. Rapid and reliable thickness identification of two-dimensional nanosheets using optical microscopy. *ACS Nano.* 2013;(Xx):10344–53.

14. Liang L, Meunier V. First-principles Raman spectra of MoS₂, WS₂ and their heterostructures. *Nanoscale*. 2014;6(10):5394.
15. Splendiani A, Sun L, Zhang Y, Li T, Kim J, Chim CY, et al. Emerging photoluminescence in monolayer MoS₂. *Nano Lett*. 2010;10(4):1271–5.
16. Scheuschner N, Ochedowski O, Kaulitz AM, Gillen R, Schleberger M, Maultzsch J. "Photoluminescence of freestanding single and few-layer MoS₂. *Phys Rev B - Condens Matter Mater Phys*. 2014;89(12):1–6.
17. Lanzillo NA, Glen Birdwell A, Amani M, Crowne FJ, Shah PB, Najmaei S, et al. "Temperature-dependent phonon shifts in monolayer MoS₂." *Appl Phys Lett*. 2013;103(9):2–7.
18. Radisavljevic B, Radenovic A, Brivio J, Giacometti V, Kis A. "Single-layer MoS₂ transistors." *Nat Nanotech*. 2011;6(3):147–50.
19. Park J, Choudhary N, Smith J, Lee G, Kim M, Choi W. "Thickness modulated MoS₂ grown by chemical vapor deposition for transparent and flexible electronic devices." *Appl Phys Lett*. 2015;106(1).

Chapter 3

Photochemical phase transition in monolayer MoS₂

3.1 Introduction

By far, chemical induced phase change by organolithium compounds is the only method compatible with large-scale monolayer TMD electronics fabrication. However, there are a number of drawbacks with this method. Two of the drawbacks of this technique include the long lithiation time (eg. a range of 2 hours to 3 days soaking at 100°C), and also the poor film quality due to the damage from the violent reaction between lithium and water.¹ The major drawback of this technique however, is that hostile organometallic chemicals that are extremely air and water sensitive and highly explosive.² Thus, this has to be used in a glove box with strict oxygen and moisture control. A researcher at UCLA recently died after using t-butyllithium when the compound reacted violently in air and set her aflame.³ The dangerous nature of these compounds and their requirement to be handled inside of a glovebox shows that there will be cost and safety issues apparent as the phase change process is scaled up. Thus, there needs to be a new, “greener” method of inducing phase change in TMDs that is absent of these dangerous organolithium compounds yet still practical and time-efficient in its usage.

To address the challenge of patterning the 1T phase with benign processes that are compatible with large-scale device fabrication, we propose a photochemical phase-change mechanism. Illustrated in **Figure 3.1b**, the electron injection to the 2H e' states is through the photo excitation of a valence band ($4d_{z^2}$) electron to the conduction band,

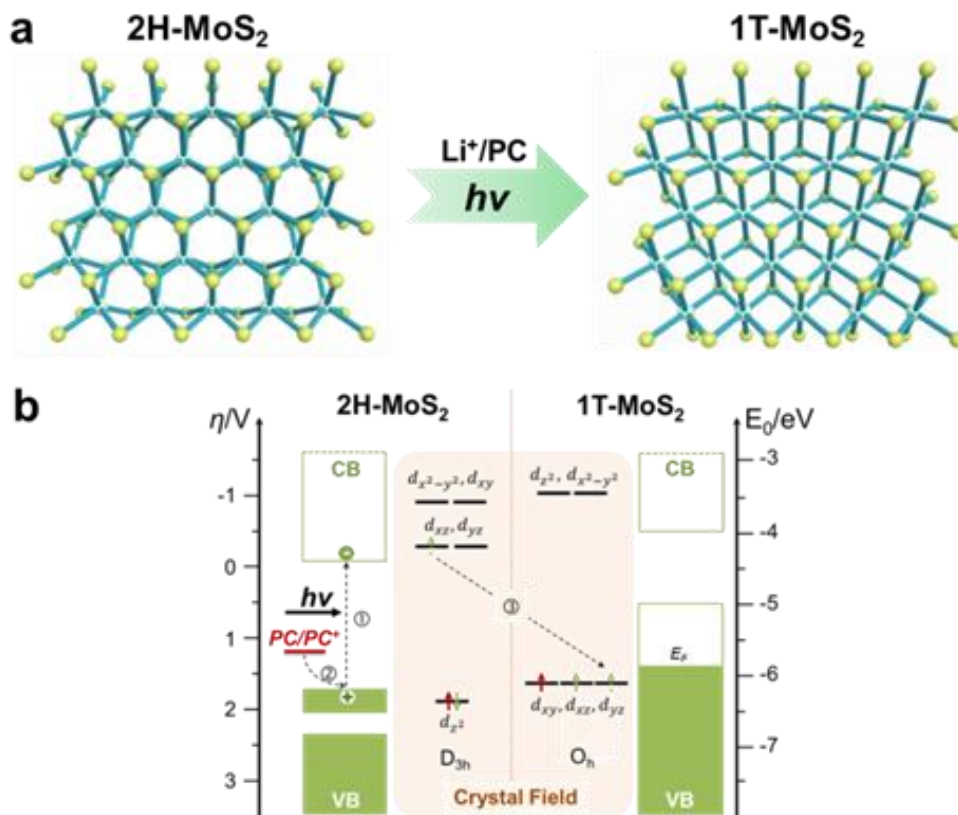


Figure 3.1: Illustration of phase transition in MoS₂ when illuminated in the presence of LiPF₆. a) Schematic showing phase transition occurring in LiPF₆-PC solution when illuminated. b) Energy band diagram indicating phase transition in the presence of excess electrons. Propylene carbonate's redox potential falls above the 2H valence band.

corresponding to the degenerate e' orbitals ($4d_{xz}$ and $4d_{yz}$). The photo-generated hole left behind in the $4d_{z^2}$ state is filled by an electron transferred from a hole scavenging molecule, whose oxidation potential is higher than 2H $4d_{z^2}$, or the top of the valence band. Effectively, this process is a photo

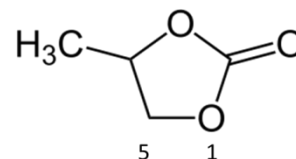


Figure 3.2: Structure of propylene carbonate

assisted reduction, in which the electron needed for the reduction of MoS₂ is supplied by the hole scavenger and the activation energy is provided by a photon. We used propylene

carbonate (PC) as the electron donor where the electron donated is most likely from the

bond between the first oxygen and carbon at position five according to literature as seen in *Figure 3.2*.⁴ The oxidation potential of PC is 1.2V vs. NHE,⁵ which converts to -5.6 eV vs. vacuum. This is slightly above the valence band of monolayer 2H-MoS₂, which is roughly around -6.5 eV.^{6,7,8} Li⁺ ions then stabilize the negative charges on reduced 1T-MoS₂.

3.2 Experimental Details

In order to characterize the success of our method, we employed a variety of characterization techniques including Raman spectroscopy, X-ray photoelectron spectroscopy, and 2D photoluminescence mapping to characterize the appearance of a 1T phase.

3.2.1 Creation of testing apparatus for use in phase change method

A freshly synthesized wafer of monolayer MoS₂ using the method described in chapter two was stored in vacuum overnight. Fresh one molar LiPF₆ in propylene carbonate was retrieved from a glovebox under argon and placed in a five milliliter vial. The SiO₂ wafer was then cut to a size of .5 inch by .5 inch and taped using kapton tape to a glass slide at the corners. It was then placed inside of a stick on plastic piece that would serve as a barrier to the atmosphere. A five microliter droplet was then placed on top of the wafer. A glass slide was immediately placed over the top and two layers of kapton tape were used to seal the glass slide in place. This would not completely prevent the exchange of oxygen with the surrounding air but had to the potential to significantly reduce it. This method was used to allow for the rapid testing of the MoS₂ domains. This structure was then used in subsequent testing for time lapsed Raman identification, XPS analysis, photoluminescence measurements and AFM.

Propylene carbonate is a benign chemical solvent. However there was a risk of HF formation from LiPF_6 from the presence of water. However, literature studies show that HF formation occurs at roughly 1 mmol/L for every 200 hours at sixty deg C in similar solutions.⁹ This is a small amount for the time limit we typically used of one hour for our measurements. We did try some control experiments using 1 M LiPF_6 solution after having been out of several days. However, several days is enough time that the amount of HF created in solution, as evident by its yellow color, washed away and damaged MoS_2 domains.

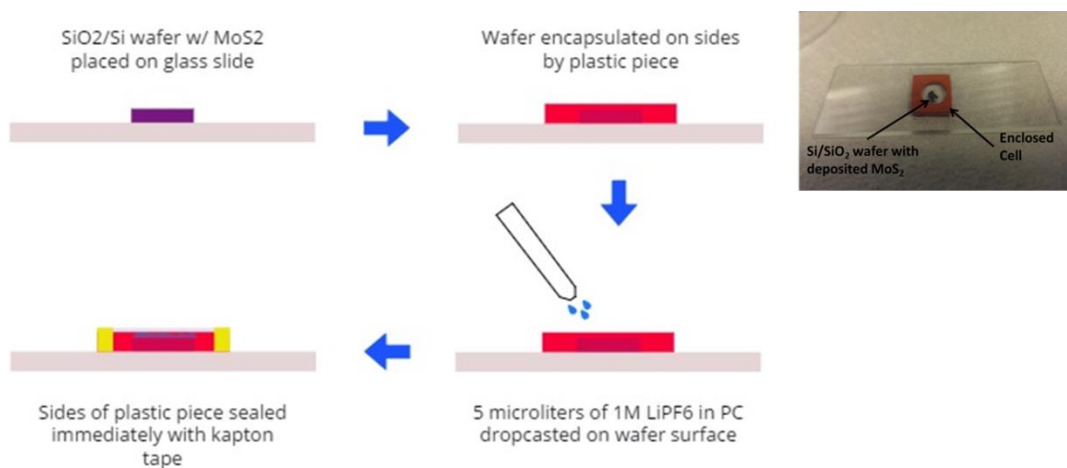


Figure 3.3: Process used to seal MoS_2 with 1M LiPF_6 in PC.

In an effort to reduce this possible danger to our experiments, we also tried creating a device that was sealed inside of the glovebox. However, we gave up on this eventually as the results from this structure did not seem to improve our results (as seen in Section 3.3.1). Li^+ is shown to be heavily dissociated in propylene carbonate even at molar concentrations of 3.29M. Thus, we knew that Li^+ would be able to bind the surface of a negatively charged MoS_2 surface if given the chance.¹⁰

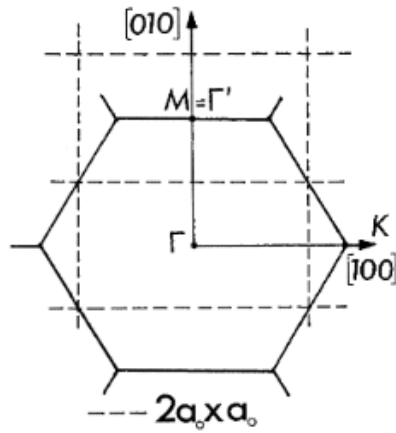


Figure 3.4: Reciprocal space diagram for 2H MoS₂.¹⁰

3.2.2 Time lapsed Raman characterization of MoS₂

Sandoval found that by chemically exfoliating MoS₂ in butyllithium solution, a superlattice was created in the 1T MoS₂ phase.¹¹ This superlattice can be seen under Raman spectroscopy by evolution of J1, J2, and J3 peaks at 150 cm⁻¹, 226 cm⁻¹ and 333 cm⁻¹ respectively. A reciprocal

space diagram can be found in Figure 3.4 that shows the relationship between the base 2H MoS₂ layer and the created superlattice. Further, there should be a drop in intensity of the major Raman modes E_{2g}¹ and A_{1g} at ~382 and ~402 cm⁻¹ respectively with an

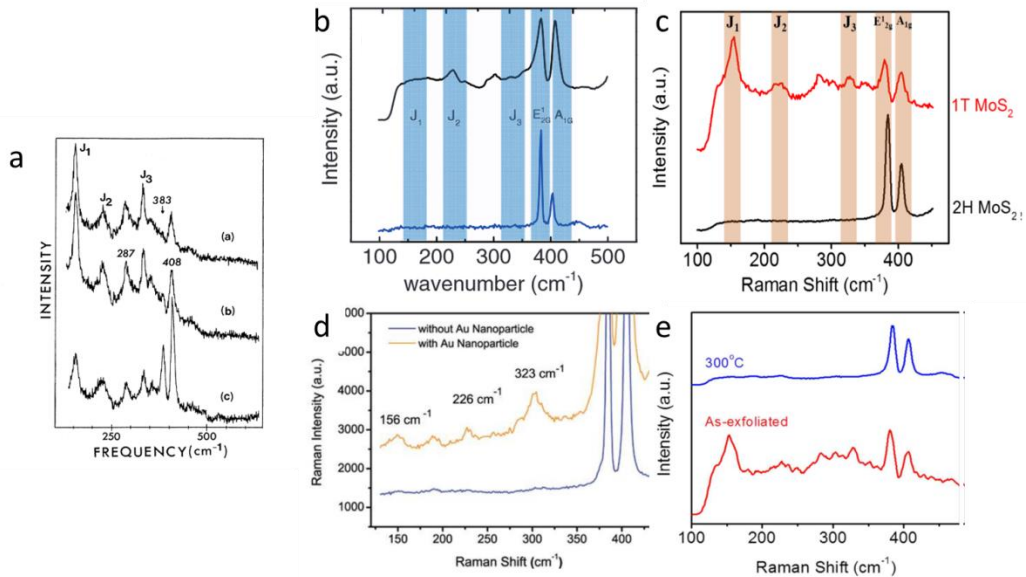


Figure 3.5: a) Original discovery of MoS₂ from exfoliated samples.⁹ b) As exfoliated 1T MoS₂.¹⁷ c) As exfoliated 1T MoS₂.¹⁸ d) 1T MoS₂ produced from electrons donated from irradiated gold nanoparticles.²⁴ e) As exfoliated 1T MoS₂.²⁵

almost complete disappearance of the E_{2g}^1 peak.¹⁰ We investigated individual domains for these characteristics.

It should be noted that these peaks are not completely consistent across all of literature as seen in *Figure 3.5*. The original recorded experiment for the evolution of these Raman peaks involved intercalation of MoS_2 in solution and showed a clear evolution of the J1, J2 and J3 peaks. Since that time, many researchers have justified the formation of 1T MoS_2 in solid film through the finding of some or all of the necessary J1, J2 and J3 peaks. In our research, we tried to match the original paper where 1T MoS_2 was first recorded.¹⁰

We used a Horiba LabRAM spectrophotometer with 10 seconds of accumulation time averaged over 3 readings. A laser power of $137 \mu\text{W}/\mu\text{m}^2$ was used using a 532 nm laser. A 1800/mm grating was used as well.

3.2.3 XPS Characterization of the 1T Phase

XPS imaging can also be used to indicate the appearance of a 1T phase in MoS_2 . After running the sample through our standard procedure, we ran it under XPS. The system we used was the Kratos AXIS Supra with an overall scan time of one hour. The aperture size used was 20 microns of which 90% of the signal came from. The X-ray beam exposure area was roughly one millimeter on each side and came from an aluminum monochromatic x-ray source. The sample was found using a 12X microscope and marked beforehand with

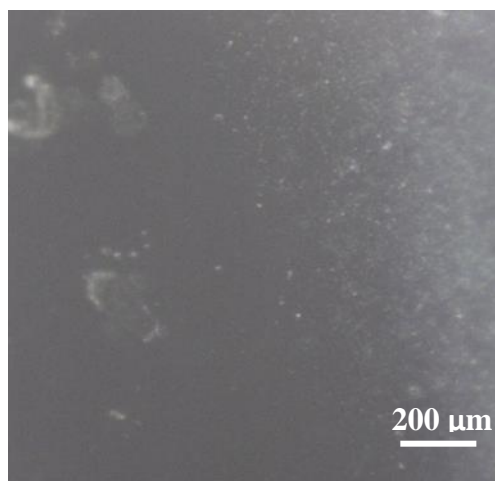


Figure 3.6: 12X microscope image in XPS.

scratches that showed the location of the changed domain. The scratches were made using a standard sewing needle attached to a micromanipulator. These scratches had to be made because the sample itself was not visible underneath the XPS microscope as the resolution was only 12X.

XPS imaging confirms that the 1T phase exists because of a shift of the Fermi level into the conduction band. The Fermi level is shifted due to band bending caused by charge transfer from the Li⁺ or n⁺ doping due to intercalated Li⁺. Coverage of Li⁺ on the MoS₂ surface causes the appearance of a new photoemission doublet which is shifted to a lower binding energy, about 1.1 eV in total for full phase transformation of a sample.¹²

3.2.4 Photoluminescence mapping of MoS₂ and atomic force microscopy

Photoluminescence quenching is an indication of the change from the semiconducting 2H phase to the metallic 1T phase. This occurs because of a shift of the Fermi level in the band structure of monolayer MoS₂. As shown in section 3.2.2, the Fermi level rests in a continuous band in 1T MoS₂. Monolayer 2H MoS₂ usually exhibits a band gap in the visible range of about 1.9 eV. However, the metallic characteristics of the 1T phase cause this to disappear.

The testing structure was placed upside down in a custom microscope setup using a HORIBA iHR550 imaging spectrophotometer and a Synapse EM CCD. A 500 mW green laser was used to illuminate individual domains. Intensity was measured at the point of contact to be about 766 $\mu\text{W}/\mu\text{m}^2$. For photoluminescence measurements, a slit of 20 microns was used. Accumulation occurred for five seconds with three accumulations averaged together with repeated accumulation provided by LabSpec 6

software. Two dimensional mapping was done at 1s accumulation per pixel using a custom LabView program. A XYZ piezo stage was interfaced with using LabView and MATLAB to change the position of the laser output in the XY plane. Power dependency data was measured in this same system by changing the input power of the laser head. Power output was measured at the point of contact with the sample using a Thorlabs Dual Channel Optical Power Meter and Energy Meter.

3.2.5 Control experiments

To further illustrate the testing of our mechanism, we subjected samples to three more testing conditions:

1. **Condition 1:** Five microliters of propylene carbonate instead of 1M LiPF₆ in propylene carbonate were used in the testing structure described in Section 3.2.1.
2. **Condition 2:** Five microliters of 1M LiPF₆ in acetonitrile instead of 1M LiPF₆

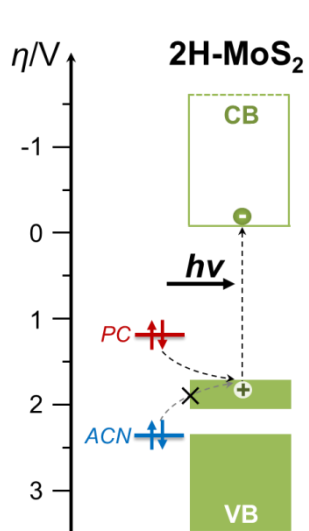


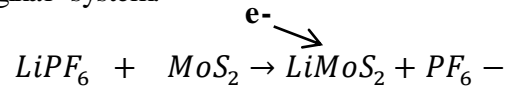
Figure 3.7: Simplified band diagram showing redox position of ACN and PC relative to valence band edge.

in propylene carbonate were used in the testing structure described in Section 3.2.1.

3. **Condition 3:** Five microliters of 1M LiPF₆ in propylene carbonate but excited using a 785 nm laser for one hour. At the end of the one hour period, a 532 nm laser was used to check the photoluminescence.

Condition 1 used just propylene carbonate solvent for the solution that would stabilize the 1T phase. The propylene carbonate solvent, as explained before, falls above the 2H valence band of MoS₂. Thus, without lithium positive ions,

there should be no stabilization of the 1T phase according to our theory. The PC can still act as a hole acceptor but recombination will still occur in the monolayer MoS₂ because there is no positive Li⁺ charge. The following equation explains what the chemical species looks like for the original system:



Condition 2 used 1M LiPF₆ in acetonitrile. LiPF₆ in acetonitrile has a redox potential that falls below the 2H valence band, making it more likely for the 2H phase MoS₂ to donate electrons to the acetonitrile instead of the other way around.^{5,13} The acetonitrile solution was prepared by mixing in 4.56 grams of LiPF₆ in thirty milliliters of propylene carbonate in a glovebox for two days at a high spin speed with the top sealed using black rubber tape. The solution was then pulled out and used immediately on a fresh MoS₂ monolayer sample. Acetonitrile evaporates extremely quickly in open air so the apparatus was taped quickly enough that there was solution trapped within the system. The redox potential of ACN and its volatility make it a poor choice for this process. Other possible solvents such as benzene would serve as poor choices because of their volatility and redox potential as well.¹⁴

Finally, for condition 3, the MoS₂ was submersed in 1M LiPF₆ in propylene carbonate but exposed to a 785 nm laser for one hour. The 785 nm laser is approximately equal to 1.58 eV. This is not enough to excite the electrons from the valence band into the conduction band given the fact that the band gap of 2H MoS₂ is ~1.9 eV. The MoS₂ was exposed for an hour at 63 μW/μm² to match other testing conditions and ensure that the material was tested long enough to completely expose the region.

3.2.6 Creation of electrical devices using 1T phase MoS₂

We wanted to create simple two terminal devices with 1T MoS₂ contacts. However, we first started with trying to change small MoS₂ sections between two gold electrode arms as we were worried about changing an entire section of MoS₂ underneath a gold contact pad would be a much more complicated process. Although, we had hoped to move onto using 1T phase contacts eventually as this would be where the main benefit was for reducing contact resistance.¹⁵ Changing an exposed section of MoS₂ while connected to a device would be simpler in design than changing the MoS₂ and then patterning over it.

We first grew MoS₂ onto a SiO₂/Si wafer as described in Chapter 2 of this document. Then photolithography recipe was followed as seen in Figure 3.6. We patterned Au/Cr (100 nm/4nm) gold pads onto a 300 nm SiO₂ wafer that was first cleaned with acetone and ethanol. The pads were 200 by 200 microns with 150 micron by 50 micron arms. Traditional lithography proved difficult as it was by pure luck using this method that MoS₂ domains would be present in between the electrode arms.

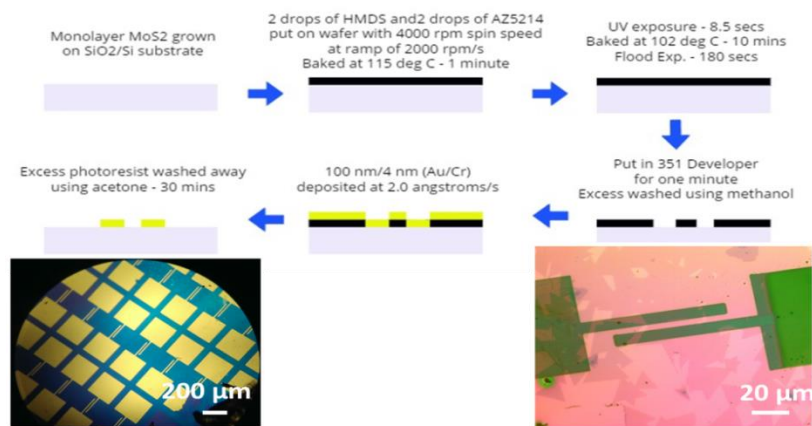


Figure 3.8: Method for creating simple MoS₂ based thin film transistors using traditional lithography.

Another method we developed was using SEM to do patterning of our electrodes. This method was similar to that described in *Figure 3.6*, however, an NNS450 SEM was

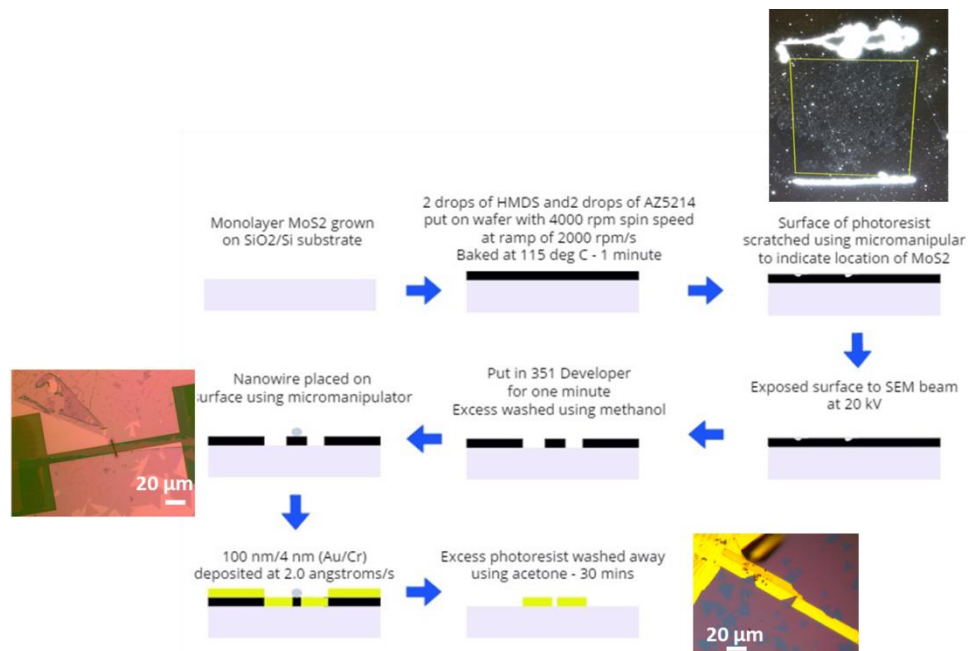


Figure 3.9: Process used to create MoS₂ two terminal devices with nanowire sized spacing.

used to expose the photoresist instead using a traditional photomask. This was done in order to get a much smaller spacing (around 100 nm, the diameter of a nanowire) between the electrode arms of MoS₂ material that we could then put through our phase change process described in Section 3.2.1. The photoresist had to be marked using a micromanipulator in order to see the location of domains in the SEM given that the photoresist itself blocked imaging of the MoS₂ domains. Then after the device had been created, we placed the device in propylene carbonate solution with LiPF₆ and a 532 nm laser was shown onto the device in the same manner as described in section 3.2.4.

3.2.7 Purely electrochemical method of phase change in monolayer MoS₂

As another test to see if phase change could be achieved for our samples, a purely

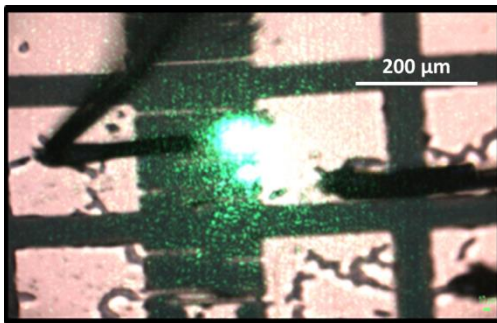


Figure 3.10: Sample under electrochemical testing.

electrochemical method was tried. This was done in response to a previous literature paper that used an electric potential to drive Li⁺ into few layer MoS₂ thus changing it into a 1T phase.¹⁶ Devices were created using the traditional lithography method as described in

section 3.2.6. Then, a West Bond model 7KEH wire bonder was used to bond two 200 by 200 micron Au/Cr (100 nm/4 nm) contact pads to an outside breadboard. This breadboard was then connected externally to a Thorlabs power supply using insulated testing wires. Testing was done by testing the Raman signal of the samples by putting the MoS₂ in 1M LiPF₆ in propylene carbonate solution while a voltage of either -1V or 1V was supplied through the MoS₂ monolayer.

3.3 Results and Discussion

3.3.1 Raman characterization

Using in-situ time-lapsed Raman studies, we were able to show that the evident peaks of the 1T phase did appear. The J3 peak was prominently shown after about fifteen minutes for this particular sample. The J2 peak seemed to already exist in the sample before the experiment even started. The J1 peak could not be seen during the experiment itself but afterwards it was found that the J1 peak existed in the sample after the experiment. These were indicative that the 1T form existed. However, as in other studies,¹⁷ quantification of the amount of 1T phase is hard to do because the signal from Raman analysis is so weak. A peak at 360 cm^{-1} did appear in solution while the J3 peak was evolving. We believe this may be attributed to a nonlinear optical process like

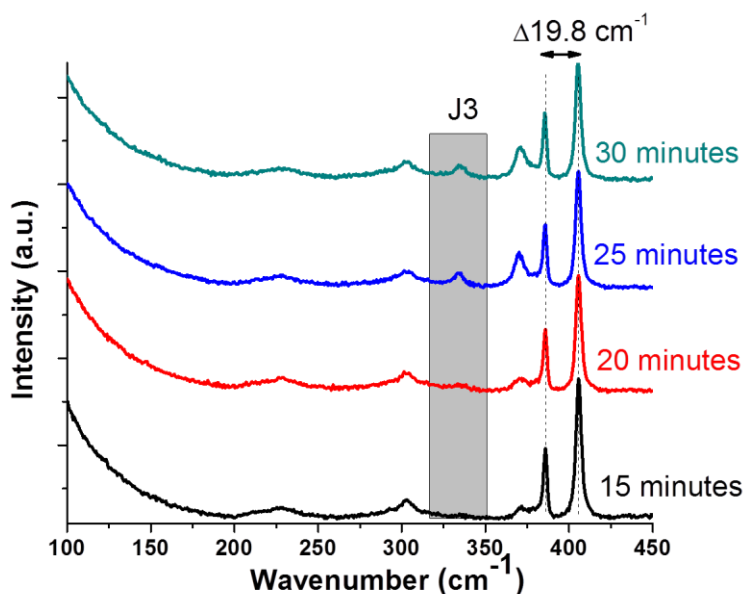


Figure 3.11: Raman spectrum showing the partial evolution of 1T phase MoS₂ under second harmonic generation. The peak has not been reported in literature to our knowledge. The peak at 300 cm^{-1} is attributed to silicon, our substrate.

We also found after washing the solution that the domain then showed the 1T characteristics were still present even after the solution was washed using pure propylene carbonate and methanol. The J3 peak was of less intensity but still present along with the J1 and J2 peaks. This indicates that the 1T phase is still present after Li⁺ is washed away as in other studies.¹⁸ Again, the amount of 1T phase could not be quantified using this method as the Raman signal is quite weak.

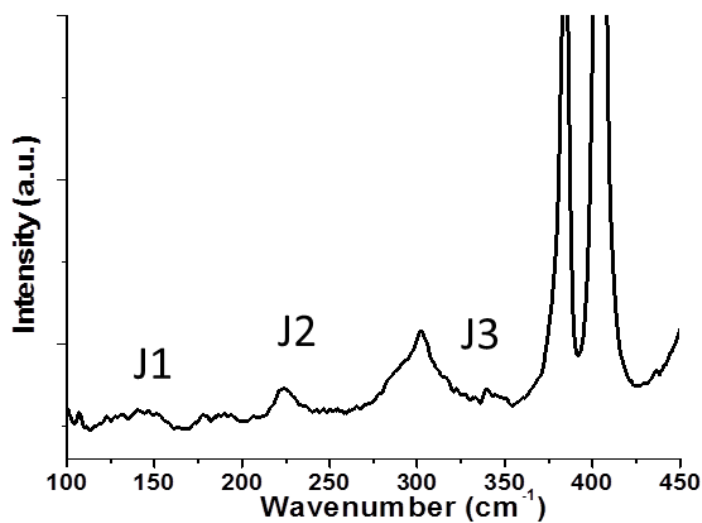


Figure 3.12: Raman spectra of relevant modes after sample was taken out of solution and washed using methanol.

3.3.2 XPS characterization

The Mo 3d region of the XPS spectrum for a monolayer MoS₂ sample can be used to confirm and quantify the amount of 1T phase MoS₂ present.¹⁹ This spectra consists of

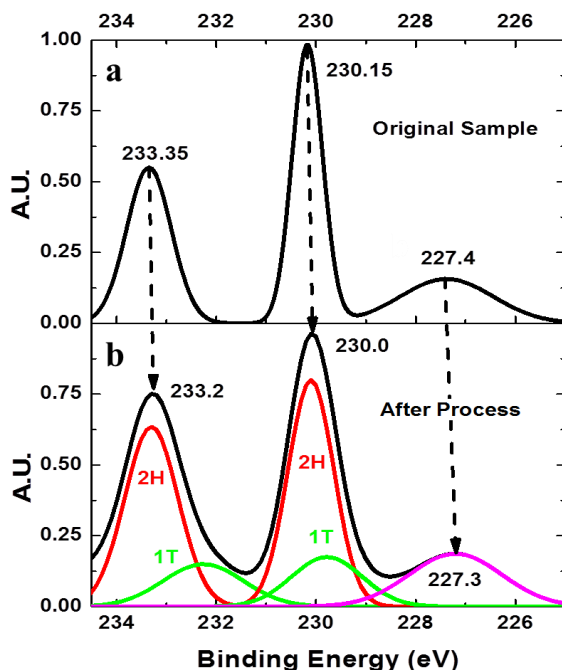


Figure 3.13: a) XPS spectra showing Mo doublet peaks before phase conversion. b) XPS spectra after partial phase change indicating a shift in these peaks to lower binding energies.

peaks around 229 eV and 232 eV according to literature that correspond to the Mo⁴⁺3d_{5/2} and Mo⁴⁺3d_{3/2} components of MoS₂ respectively.²⁰ The peaks were normalized in MATLAB to the highest intensity present. Our XPS characterization does not reveal a full phase transformation for the area examined as evidenced by the obviously overlapping peaks that appear at these positions. This makes sense as we did not expect the full area to be phase transformed but rather only a region of about three microns in diameter as that is the size of the laser spot used to transform these domains. As stated in

the methods, the aperture size used was 20 microns with 90 percent of the signal coming

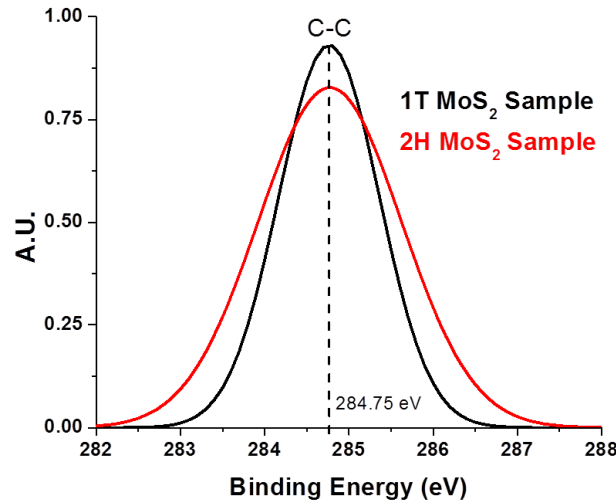


Figure 3.14: Adventitious carbon peak used as a reference. from this area. A three micron size laser spot size is fifteen percent of a twenty micron area so it makes sense that our data indicates about a fifteen percent phase conversion.

Figure 3.14 also shows that the carbon peak for both samples is at the same location indicating that there is an actual shift in the molybdenum orbital peak centers, despite it only being .15 eV. This carbon data was taken at the same time that the original XPS data was taken. The adventitious carbon peak at approximately 284.5 is commonly used a reference peak in XPS and should not be affected by the change to the 1T phase.²¹ The peak centers were found using the peak analyzer option in Origin Lab.

3.3.3 Photoluminescence mapping of MoS₂ and atomic force microscopy

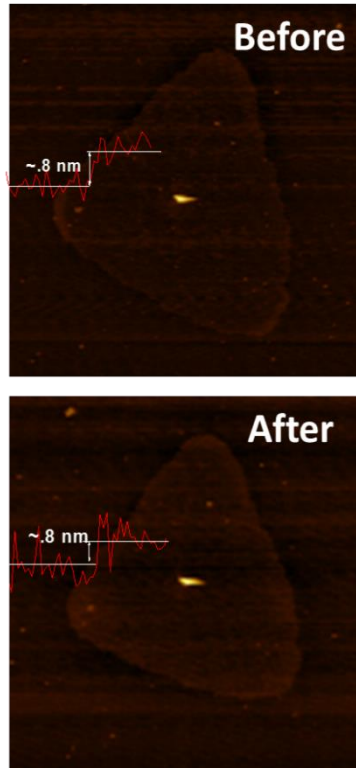


Figure 3.15: AFM image of monolayer MoS₂ domain before and after phase change process.

Atomic force microscopy indicates that the sample is not damaged after exposure to the laser in solution when exposed to a 532 nm laser. Under such a low power ($137\text{-}766 \mu\text{W}/\mu\text{m}^2$) there was no laser ablation. MoS₂ flakes seem to not be laser ablated below about $80 \text{ mW}/\mu\text{m}^2$ so the flake did not show damage from the laser.²² There is a slight increase in surface roughness that is apparent from the inability to fully remove all of the LiPF₆ but this does not affect the overall height of the material. Unfortunately, we were unable to measure the temperature of the laser at the MoS₂ surface in

solution.

As stated before, the 1T phase of MoS₂ is a metallic one. There is a clear drop in photoluminescence as a result of this. Using 2D mapping over time, we found that there was a clear drop in photoluminescence for nearly the entire domain.

Figure 3.16 shows the drop in photoluminescence over time for one sample at a power intensity of $766 \mu\text{W}/\mu\text{m}^2$. Time at which phase change occurred seemed to vary

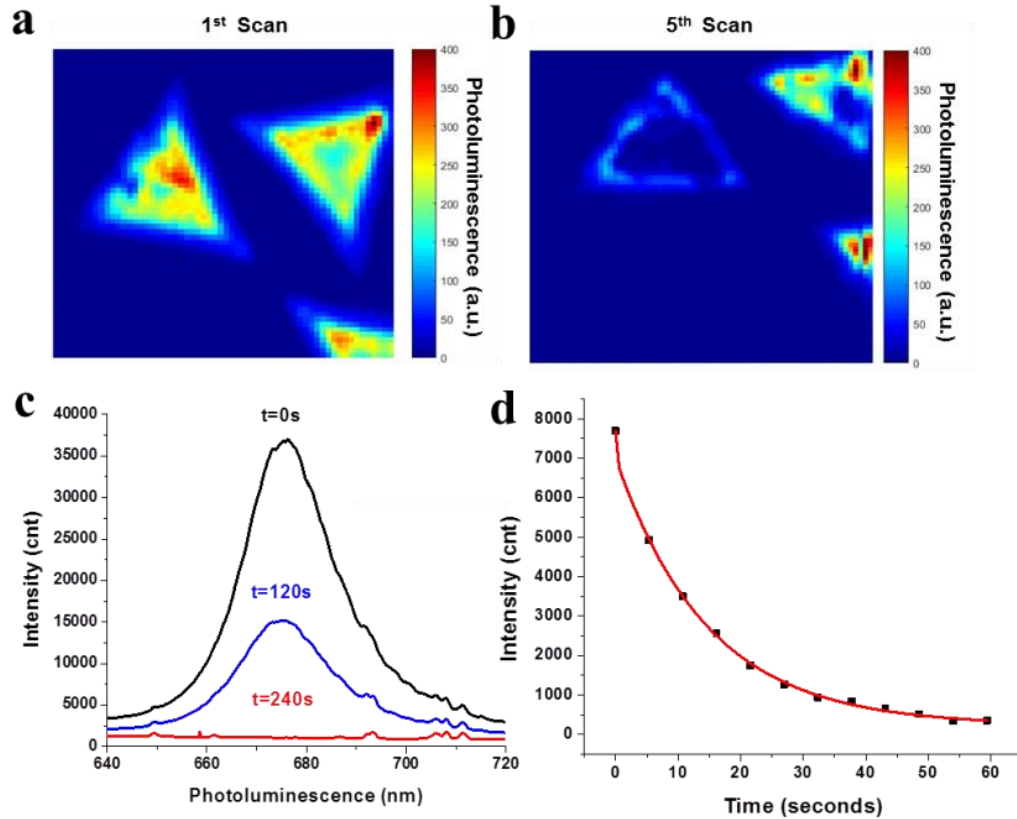


Figure 3.16: a) 2D mapping of PL of monolayer domain at start. b) 2D mapping of PL after fifth scan. c) Intensity drop in PL for a monolayer sample. d) Tail end of graph in c showing exponential relationship.

for samples and we believe is purely dependent on the sample quality for the same laser power density. It can be seen that exact dimensions between the domain in the AFM images and the photoluminescence mapping are not exactly the same. This is because CVD grown MoS_2 inherently has point defects that make samples different from each other and as stated before the shape of the edges can be affected by either being sulfur or molybdenum terminated.²³ The end of the drop in photoluminescence at **Figure 3.16d** is shown to be exponential in nature.

The below scans show the complete scans between the first and fifth scans. It can be seen that there is slight lateral drift from the microscope. This however, did not affect the phase change process. Unfortunately, there were also software errors during the 2nd and 4th scans that affected the produced images but not the overall process. All images were normalized to each other to show photoluminescence values actually dropped over time.

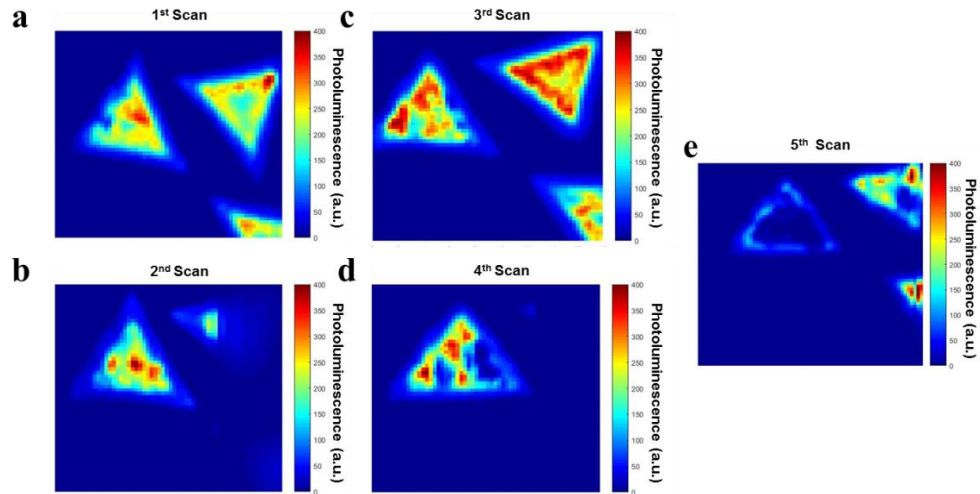


Figure 3.17: Full scans of sample in Figure 3.13. There is some drift evident as the sample is scanned.

It can be seen from this that there is a drop in photoluminescence in 240 seconds for one sample yet evolution of the necessary Raman peaks did not appear until after twenty-five minutes for the sample used in section 3.2.1. As stated before, we believe this is due to the differences in the MoS₂ domains produced using our system. We could not clearly define the relationship between the quality of films and the time at which phase change would occur. We theorize that point defects may interfere with the travel of holes and electrons throughout the MoS₂-PC system. We did find a rough power dependence relationship in which phase change would occur as shown in *Figure 3.18*. We get an almost linear fit from this data. Clearly, more research needs to be done to

elucidate how film quality affects the ability of individual molecules to change phase and if a more accurate relationship can be determined between parameters.

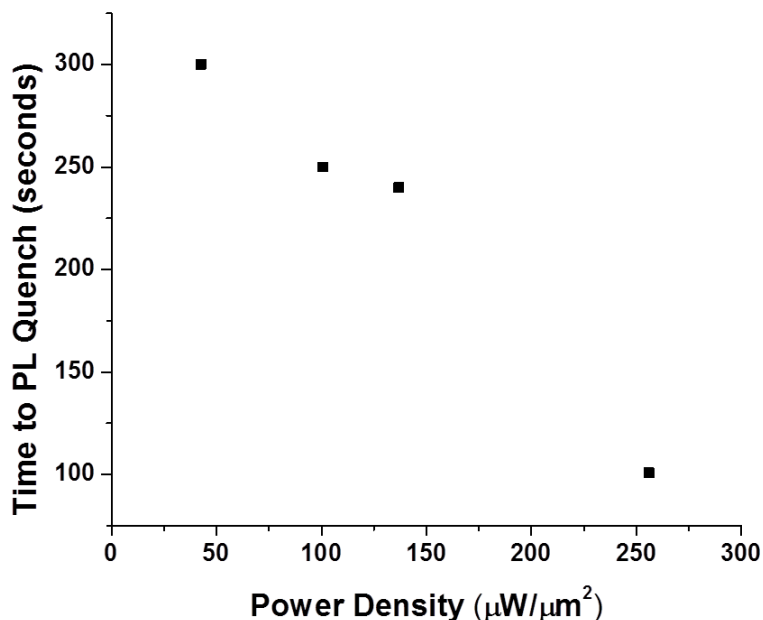


Figure 3.18: Time at which PL was quenched versus the output power density.

3.3.4 Control experiments

Conditions 1, 2 and 3 resulted in only a slight drop in photoluminescence over the period of an hour. This could be attributed to drift in the z direction from either slight loss of solution or the stage moving itself. In condition 1, the propylene carbonate without LiPF_6 did not have the ability to stabilize a 1T phase as expected. Condition 2 resulted in almost no drop as well because the acetonitrile did not have the proper redox potential to act as a hole acceptor. Some of the acetonitrile did evaporate from the system but there was still most left at the end of the test condition. Condition 3 resulted

in almost no drop in photoluminescence as well. The 785 nm (1.56 eV) laser did not have enough energy to change the 2H MoS₂ to the 1T phase.

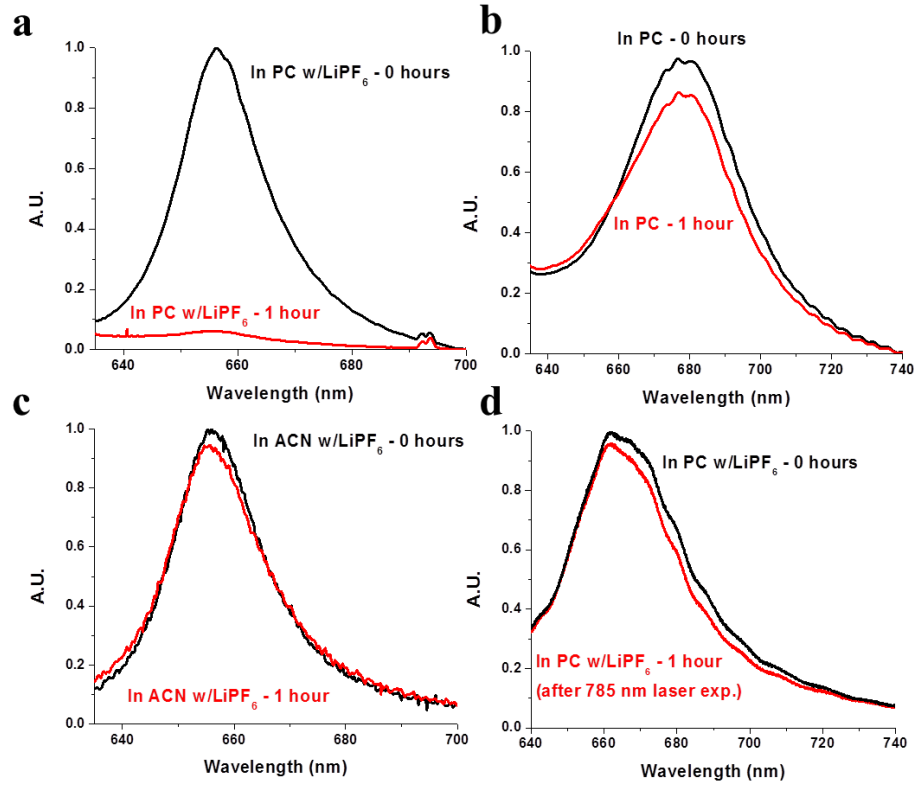


Figure 3.19: a) Typical drop in PL seen when using 1M LiPF₆ in PC. b) PL after 1 hour exposure to just PC. c) PL after 1 hour exposure to 1M LiPF₆ in ACN. d) PL after 1 hour exposure to a 785 nm laser in 1M LiPF₆.

Curiously, under just PC we also saw a color change in some of our samples after being exposed to a 532 nm laser at a power density of 137 $\mu\text{W}/\text{m}^2$ even for just five seconds. There is a slight drop in the A exciton with some attributed to drift. In addition, there was an increase in the response at five hundred nanometers. We currently do not know why this has occurred as a result of using just propylene carbonate absent lithium hexafluorophosphate. Further investigation will need to be done into this phenomenon as we believe it is not currently reported in the literature.

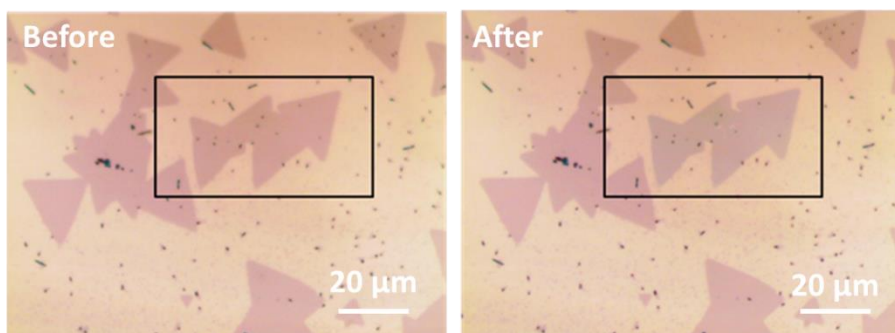


Figure 3.20: (Left) Dry MoS₂ domains. (Right) MoS₂ domains after exposure to a 532 nm laser for five seconds.

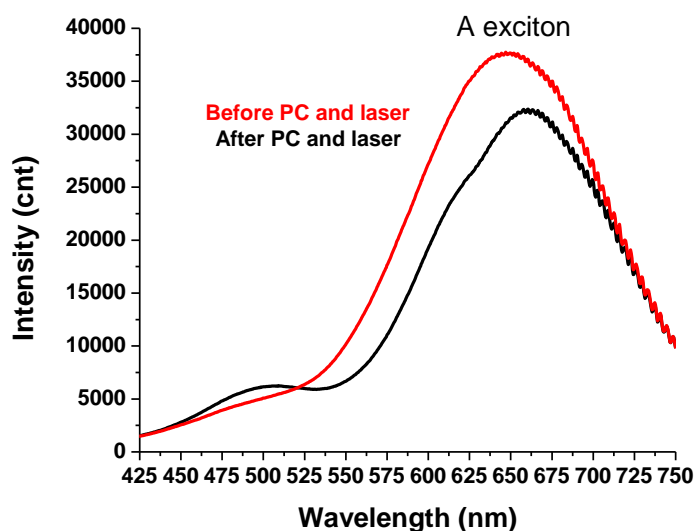


Figure 3.21: PL Before (red) and after (black) being exposed to a 532 nm laser in PC. There is a slight drop in the A exciton and an increase in the B exciton.

3.3.5 Creation of electrical devices using 1T phase MoS₂

Our preliminary devices showed a drop in overall resistance for a two terminal device. We managed to create two terminal devices and then tested the overall resistance across these devices. The resistance did drop for the devices we did create, however, we did not exactly trust the results as we believe that the devices may have had better resistance from the contamination of the sample itself. Also, though the resulting

resistance was almost one thousand times smaller, an overall resistance of $.1\text{M}\Omega$ is still extraordinarily high compared to what is needed for commercial devices. It is possible that the LiPF_6 itself may have increased the conductivity of our sample and we cannot currently rule this out. There needs to be further studies into the incorporation of devices using our photochemical phase change method.

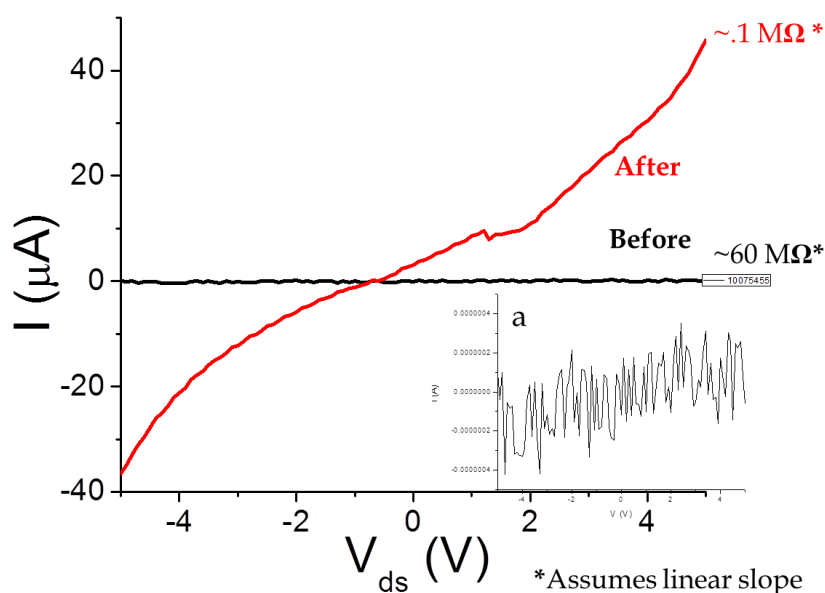


Figure 3.22: An IV curve of the same device before and after being exposed to a 532 nm laser for one hour in 1M LiPF_6 solution. The inset at a shows that the before curve was not perfectly flat.

3.3.6 Purely electrochemical method of phase change in monolayer MoS_2

Using this method, we unfortunately did not see a change in the Raman signal of our monolayer. There was a slight change in the heights of the E_{2g}^1 and A_{1g} intensities but this was most likely because of drift or evaporation of the propylene carbonate solution. Voltage was increased up to 3V positive bias and -2.2V negative bias but this began to destroy the gold pads without causing any change in the Raman signal of the

monolayer. The phase change test for this particular sample was only up to four minutes, thus, there may be a different result if the test is ran longer.

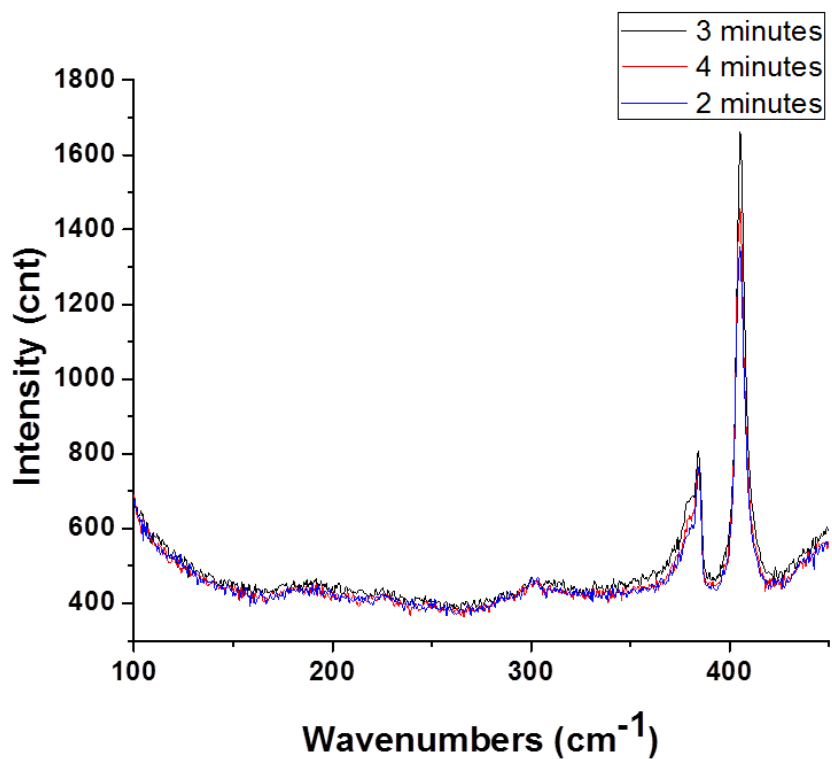


Figure 3.23: A Raman spectra of MoS₂ in between two electrode arms while being exposed to MoS₂ in 1M LiPF₆ in PC solution. This graph shows the intensity of the Raman spectra at 1V.

3.4 References

1. Voiry D, Salehi M, Silva R, Fujita T, Chen M, Asefa T, et al. "Conducting MoS₂ nanosheets as catalysts for hydrogen evolution reaction." *Nano Lett* . 2013;13(12):6222–7.
2. Effects PH. MSDS for (n-Butyllithium). 1901;
3. Kemsley J. Learning from UCLA. *C&EN*. 2017;87(31):1–23.
4. Xing L, Borodin O, Smith D, Li W. "A density function theory study of the role of anions on the oxidative decomposition reaction of propylene carbonate." *J Phys Chem C*. 2011;13896–905.
5. Kanamura K. "Studies on electrochemical oxidation of nonaqueous electrolytes using in situ fir spectroscopy." *J Electrochem Soc* . 1995;142(5):1383.
6. Schlaf R, Lang O, Pettenkofer C, Jaegermann W. "Band lineup of layered semiconductor heterointerfaces prepared by van der Waals epitaxy: Charge transfer correction term for the electron affinity rule." *J Appl Phys* . 1999;85(5):2732–53.
7. Sup Choi M, Lee G-H, Yu Y-J, Lee D-Y, Hwan Lee S, Kim P, et al. "Controlled charge trapping by molybdenum disulphide and graphene in ultrathin heterostructured memory devices." *Nat Commun* . 2013;4:1624.
8. Furchi MM, Pospischil A, Libisch F, Burgdorfer J, Mueller T. "Photovoltaic effect in an electrically tunable van der Waals heterojunction." *Nano Lett* . 2014;14(8):4785–91.
9. Lux SF, Lucas IT, Pollak E, Passerini S, Winter M, Kostecki R. "The mechanism of HF formation in LiPF₆ based organic carbonate electrolytes." *Electrochem commun* . 2012;14(1):47–50.
10. Kondo K, Sano M, Hiwara A, Omi T, Fujita M, Kuwae A, et al. "Conductivity and solvation of li + ions of lipf 6 in propylene carbonate solutions." *J Phys Chem B* . 2000;104(20):5040–4.
11. Jiménez Sandoval S, Yang D, Frindt R, Irwin J. "Raman study and lattice dynamics of single molecular layers of MoS₂." *Phys Rev B*. 1991;44(8):3955–62.
12. Papageorgopoulos CA, Jaegermann W. "Li intercalation across and along the van der Waals surfaces of MoS₂ (0001)." *Surf Sci*. 1995;338(1):83–93.
13. Seo DM, Borodin O, Han S, Boyle PD, Henderson WA. "Electrolyte solvation and ionic association ii . Acetonitrile-lithium salt mixtures : highly dissociated salts."

2012;159(9):2–13.

14. Merkel PB, Luo P, Dinnocenzo JP, Farid S, York N. "Accurate oxidation potentials of benzene and biphenyl derivatives via electron-transfer equilibria and transient kinetics." 2009;(d):5163–73.
15. Mohite AD, Chhowalla M. "Phase-engineered low-resistance contacts for ultrathin MoS₂ transistors." *Nat Mater*. 2014;13(December).
16. Xiong F, Wang H, Liu X, Sun J, Brongersma M, Pop E, et al. "Li intercalation in mos₂: in situ observation of its dynamics and tuning optical and electrical properties." *Nano Lett*. 2015;15(10):6777–84.
17. Kappera R, Voiry D, Yalcin SE, Jen W, Acerce M, Torrel S, et al. "Metallic 1T phase source/drain electrodes for field effect transistors from chemical vapor deposited MoS₂." *APL Mater* . 2014;2(9):92516.
18. Kappera R, Voiry D, Yalcin SE, Branch B, Gupta G, Mohite AD, et al. "Phase-engineered low-resistance contacts for ultrathin MoS₂ transistors." *Nat Mater* . 2014;13(12):1128–34.
19. Eda G, Yamaguchi H, Voiry D, Fujita T, Chen M, Chhowalla M. "Photoluminescence from chemically exfoliated MoS₂." *Nano Lett*. 2011;11(12):5111–6.
20. Papageorgopoulos CA. "Li intercalation across and along the van der Waals surfaces of MO &(0001)." *Surf Sci*. 1995;338:83–93.
21. Xiao Z, Jin S, Pang M, Liang C. "Conversion of highly concentrated cellulose to 1,2-propanediol and ethylene glycol over highly efficient CuCr catalysts." *Green Chem* . 2013;15(4):891.
22. Barkelid M, Goossens AM, Calado VE, Zant HSJ Van Der, Steele GA. "Laser-thinning of mos₂: on demand generation of a single-layer semiconductor." *Nano Lett*. 2012;1–6.
23. Liu Y, Ghosh R, Wu D, Ismach A, Ruoff R, Lai K. "Supporting information mesoscale imperfections in mos₂ atomic layers grown by vapor transport technique." *Nano Lett*. 2014;
24. Kang Y, Najmaei S, Liu Z, Bao Y, Wang Y, Zhu X, et al. "Plasmonic hot electron induced structural phase transition in a mos₂ monolayer." *Adv Mater* . 2014;26(37):6467–71.
25. Voiry D, Salehi M, Silva R, Fujita T, Chen M, Asefa T, et al. "Conducting mos₂

nanosheets as catalysts for hydrogen evolution reaction." Nano Lett. 2013;

Chapter 4

An epitaxial, ultra-thin gold coating as a barrier to prevent oxidation of silver nanowires

4.1 Introduction

Silver nanowire networks have been proposed as an alternative to indium tin oxide (ITO) as an electrode material for flexible electronics. Silver nanowires have

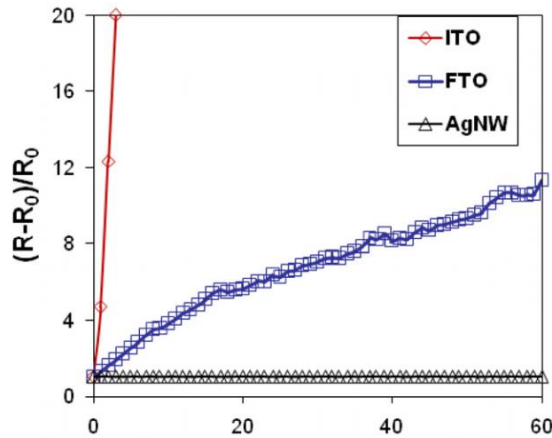
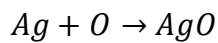
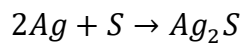


Figure 4.1: A comparison of ITO, FTO and Ag NW network bent to 5 mm.

excellent intrinsic chemical, optic and electrical properties, because of their high crystallinity, high surface-to-volume ratio, and atomically flat surface.^{1,2} Silver nanowires are the most conductive metal in existence (~50 times more conductive than ITO).³ They are able to bend up to 5 mm up to ten

thousand cycles without degradation in performance when put into networks on flexible surfaces. Unlike ITO, they can be fabricated using solution based processes directly onto flexible substrates without the need for transfer from another medium either through roll to roll fabrication.⁴ Because of these cheap solution based processes, even though silver is more expensive per kilogram than ITO (approximately \$765 kg⁻¹ versus \$600 kg⁻¹), the processing costs severely offset the material cost.³

Thus, Ag nanowires hold promise for applications such as transparent and flexible displays, solar cells, chemical/biological sensors, photonic circuits and scanning probe microscopy^{5,6,7}. However, their susceptibility to damage from oxidation and sulfurization has limited their commercialization. The structure and chemical properties of Ag nanowires are can be altered when exposed to water, acids, oxidative agents and even air environments. In air environments, they corrode in the following manner:⁸



Heat and UV irradiation can play a damaging role as well. This damage can be suppressed by a surface protective coating such as a polymer (PDMS⁵, PMMA or PES⁶), or silica coating.⁷ However, this reduces the transmittance of the silver nanowires themselves and adds to light absorbance. Also, the high resistance of the polymers or silica reduce the overall conductivity. Researchers are also attempting to coat metal nanowire networks using atomic layer deposition.⁹ Unfortunately, this adds to the material processing cost through expensive cleanroom equipment needed to do this process. These various methods have improved the stability of silver nanowire networks to some degree but it is still a great challenge to keep their unique plasmonic properties and high electrical conductivity in a real world environment over time.

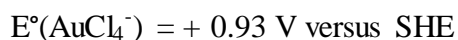
It has been proposed more recently to coat silver nanowires with gold to not only protect them from atmospheric corrosion but to maintain their unique plasmonic properties. This has been previously done on nanoplates to protect their stability in biosensing.^{5,6} It has also been done on silicon nanowires for use as an anode in batteries and silver nanowires to function as electrodes as well.^{10,11} Gold and silver have lattice

constants of 4.97 angstroms and 4.77 angstroms respectively, meaning that gold has the ability to conformably coat silver because of little lattice mismatch (.16%).¹² In addition, gold is highly biocompatible and stable in the open atmosphere.¹³ Thus, it was seen as a good choice to use gold as a coating for silver nanowires.

Ultra-long (>100 micron in length) silver nanowires can be created using a standard procedure found in the literature.¹⁴ Gold can be conformably coated onto silver nanowires using a solution based process that overcomes galvanic replacement. Galvanic replacement is the act of oxidizing a sacrificial template metal when surrounded by ions of a metal that have a higher reduction potential and then plating that metal onto the surface of the template metal. This is used in a number of papers to create various shapes including hollow nanowires, nanospheres, nanoprisms and nanocubes.¹⁵ Also, it can cause a non-uniform deposition of the metal ions to occur because the reaction is locally limited to high energy sites.⁵ However, if one wants to coat a metal surface without sacrificing the template metal, then galvanic replacement has to be overcome.

We were able to coat our silver nanowires with gold and overcome galvanic replacement through three advantages:

1. Reduce the reduction potential of the Au complex used in the reaction:⁵



2. Use polyvinylpyrrolidone (PVP) in the system to act as an additional ligand to stabilize silver. This works because of the strong coordination between the oxygen and nitrogen atoms of the PVP ring and silver surface.

- Use diethylamine to eliminate the energy difference for etching/deposition between the different facets of silver. This is because PVP preferentially absorbs to (100) facets.⁵

Once both silver nanowires and gold coated silver nanowires are formed in solution, they can then be formed into meshes. Inherently, silver nanowire networks do not form meshes well under drop casting though. This is

Table 4.1: Reported values for individual nanowire junctions from various literature sources.²³

author	year	R_{jxn} (Ω)	method
Lee <i>et al.</i> ²¹	2008	1–100	fitting simulation to experiment
Hu <i>et al.</i> ⁵	2010	450	four-probe measurement
Garnett <i>et al.</i> ²⁷	2012	$\sim 1 \times 10^4$	two-probe measurement
Mutiso <i>et al.</i> ³¹	2013	$\sim 2 \times 10^3$	fitting simulation to experiment
Song <i>et al.</i> ³²	2014	185	two-probe measurement

because of the high wire to wire contact resistance at the nanowires junctions.¹⁶ Thus, drop casting silver nanowire networks typically does not create usable networks as it disperses nanowires randomly, causing a large number of junctions to form and does not do anything to improve the connection at the nanowire junctions. Researchers have gone down three main routes to improve these types of meshes:

- Make nanowires longer through synthesis processes to reduce the amount of connections between individual nanowires and maximize the amount of longitudinal traveling of current along the nanowire where resistance is lowest¹⁷
- Positioning the nanowires into a more grid like fashion using roll to roll processes to reduce the amount of connections between nanowires¹⁸

3. Improving nanowire junctions by physically welding the nanowires together through plasmonic nanowelding, pressure annealing or even humidity assisted annealing^{16,19,20}

In this project, we first created ultra-long gold coated silver nanowires. Then, after filtering them with vacuum assisted filtration, they were pressed onto flexible PET and glass with gold contact pads to see their resistance to corrosion over time versus the bare silver nanowire controls.

4.2 Experimental Details

4.2.1 Creation of gold coated silver nanowires

In order to first create the silver nanowires, in a typical synthesis, ten milliliters of ethylene glycol (EG) was added to a round-bottom flask (one hundred milliliter, equipped with a magnetic stirring bar); the flask was then suspended in an oil bath and heated at 185 °C for fifteen minutes. Then, sixty microliters of copper chloride (CuCl_2 , 0.0073M) was injected to this ten milliliters of EG solution. After fifteen minutes, ten milliliters of AgNO_3 solution (0.15M, in EG, freezing for ten minutes before use) and ten milliliter of PVP solution (0.45 M as calculated in terms of the repeating unit, in EG) were added dropwise to the heated EG solution at a pace of 200 $\mu\text{l}/\text{minute}$. The growth of nanowires was monitored by sampling small portions of the reaction mixture every ten minutes. Mild stirring with 400 rpm was maintained throughout the whole process. The final product was diluted with ethanol (eight \times by volume) and centrifuged at 2000 rpm for twenty minutes at least four times. In order to separate silver particles with silver nanowires completely, the sample was treated continually by decreasing centrifugation speed or increasing centrifugation time and then a small drop was checked under the

microscope. This centrifugation procedure could be repeated several times until the supernatant became colorless.

In order to then coat the silver nanowires with gold, one milliliter of the above solution of Ag nanowires were dispersed into nine milliliter of H₂O, then two milliliters of PVP, 237.5 microliters of ascorbic acid (0.018 g/mL) and fifty microliters of diethylamine were added to the nine milliliters of silver nanowire- dispersed aqueous solution (0.0061 g/ml), respectively. A separate growth solution for Au precursor was prepared by incorporating 400 microliters (0.0061 g/ml), eighty microliters of KI (0.0068 g/ml) and twenty microliters of HAuCl₄ (0.002 g/ml) in three milliliters of H₂O. By using a syringe pump, 1.2 milliliters of Au growth solution was slowly added into the solution of silver nanowires at a pace of 0.05 ml/min to deposit a thin layer of Au on the surface of the Ag nanowires. The gold coated silver nanowire (Ag@Au) nanowires were collected by centrifugation, washed with H₂O twice and stored in H₂O for further use after filling a fifty milliliter vial to the brim to prevent excess air exposure.

As described in the following chapters, nanowires were spread across glass slides. Scanning electron microscopy images along with EDS mapping and accompanying line scan were taken of the samples using a SEM FEI NNS450 at twenty kV. High resolution tunneling electron microscopy images were taken using a Tecnai12 TEM.

4.2.2 Drop casting of nanowires onto flexible substrates

The first test for creating nanowire networks was simple drop casting of nanowire solution on glass slides in various amounts ranging from five microliters to twenty five microliters. This was done to see if workable nanowire networks could be created using the simplest process available. Standard glass slides from Fischer Scientific were used

as the substrate. These were cleaned by washing with acetone and then ethanol and then a N₂ blow gun at a high rate to quickly dry the surface. Both silver nanowire solution and gold coated silver nanowires were then extracted from solution and dropped onto glass slides in various amounts.

4.2.2. Plasmonic nanowire welding

Because initial nanowire based solutions did not produce workable results, nanowire based plasmonic welding was tried to improve contact points between individual nanowires. Under medium vacuum at two torr, a simple 100W bulb was shined onto silver nanowire networks inside of a glass CVD tube. The illumination took place from a range of 30 seconds to 30 minutes.

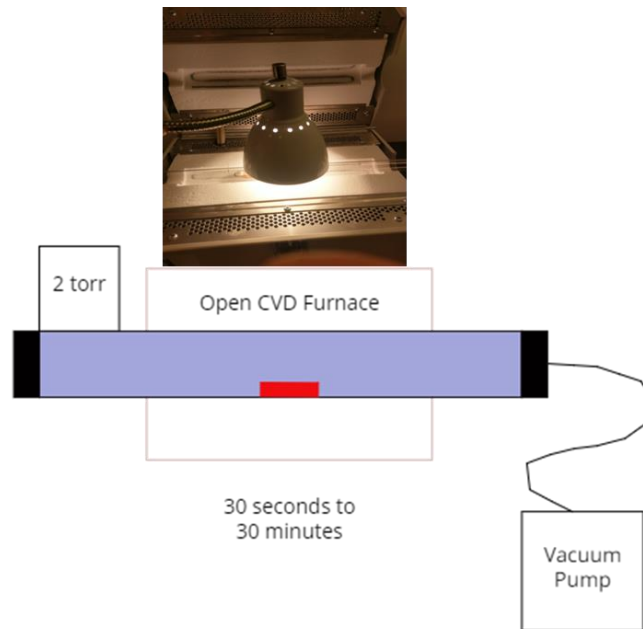


Figure 4.2: Setup used to perform plasmonic nanowelding on silver nanowire mesh.

4.2.3. Press on filter method

It was found that pressure could be a better way to make usable networks in line with current literature.²¹ Glass slides were solvent washed and sonicated in both acetone and ethanol for twenty minutes each. They were then blow dried using a nitrogen gun. 100nm/4nm (Au/Cr) was deposited onto glass slides using a copper mask in a custom Angstrom Engineering thermal evaporator system. Chrome and gold were deposited at a rate of 2.0 Angstroms/second to ensure smoothness. Devices were then stored in vacuum until deposition was ready to occur.

Ag@Au nanowires were diluted with toluene and sonicated for ten minutes to form a homogeneous solution. The transparency film was prepared by filtering down the nanowires from the dispersion on to a nitrocellulose porous membrane with 220 nm of pore size via vacuum filtration. Ten microliters of solution was used for this membrane step in order to keep the amount of nanowires used consistent. Then the nanowire network was transferred completely on to a transparent substrate (PET, glass slides with gold contact pads or PDMS) by applying finger pressure to the back side of the membrane using a circular stainless steel disk about the size of the filter. The amount of nanowire solution was kept the same as it was drop casted on every filter.

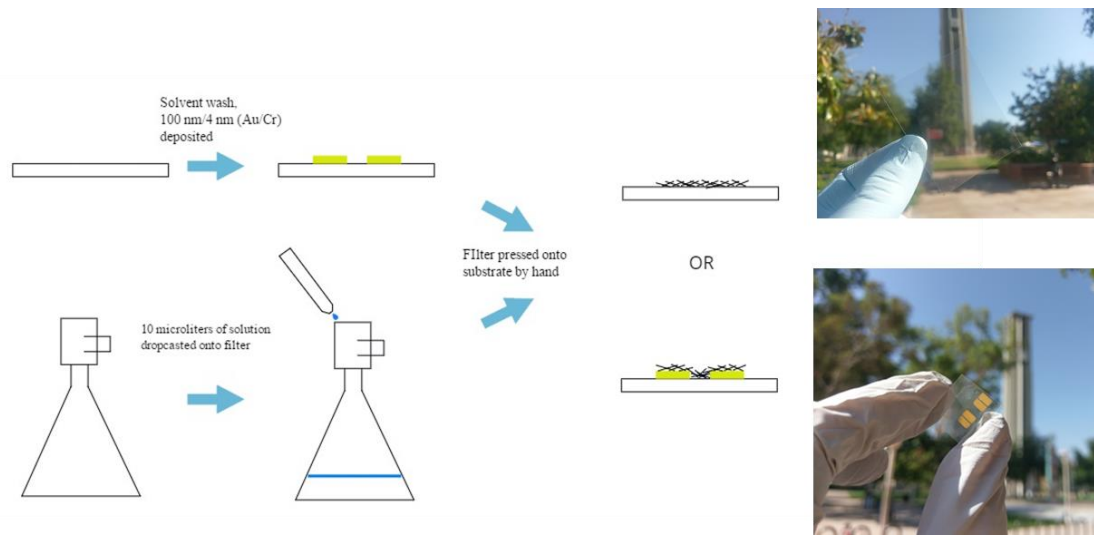


Figure 4.3: Process used to create nanowire mesh based devices

Three different conditions of samples were created using this method:

- a) **Condition 1:** A filter with nanowire solution was pressed onto flexible PET substrates with silver paste contacts. Silver paste was spread across each end of the

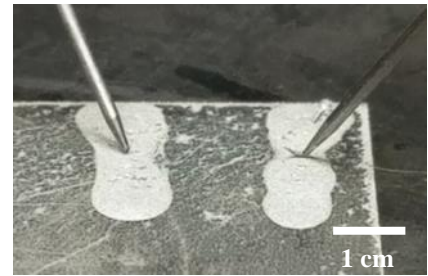


Figure 4.4: AgNW mesh on PET under probe station.

visible network using a small brush. This was then allowed to dry in open air. These testing structures were stored in a petri dish inside of a plastic bag open to the atmosphere.

- b) **Condition 2:** A filter with nanowire solution was pressed onto a glass slide substrate with 4 nm/100 nm (Cr/Au) contacts already present on the surface. This was then allowed to dry in open air. After drying the device was placed into a Thermofisher Heratherm oven at 80 deg C.

c) **Condition 3:** A filter with nanowire solution was pressed onto a glass slide substrate with 4 nm/100 nm (Cr/Au) contacts already present on the surface. This was then allowed to dry in open air.

After drying the device was placed inside of a tin can that sat inside of a larger aluminum can. A mass of metal foil was put at the bottom to let the tin can sit on top. Then

five hundred milliliters of water were filled into the bottom. An Acurite humidity



Figure 4.5: Testing chamber for 80 deg C/100% humidity testing condition.

sensor was used to test the relative humidity of the chamber inside of the oven and was found to reach 99% which was rounded to 100% for our data because the sensor could not support three digits although it was obvious full saturation had occurred.

d) **Condition 4:** Several filters with differing amounts of Ag@Au nanowire solution was pressed onto a flexible PET substrate. These substrates were then analyzed using a Varian Cary 50 UV/Vis spectrophotometer in the visible range for their transparency.

4.2.4 Resistance measurements

Each of the testing apparatuses were taken out of their testing environments at various intervals ranging from every twelve hours to every week as the test went on. Resistance of the devices were measured using a Signatone CM200 probe station and Agilent 4155A Semiconductor Parameter Analyzer by placing the probes on the contact pads and ran between -1V to 1V. Overall resistance was measured from the inverse of

the slope of the IV curve as there was always ohmic curves present until the devices broke.

Access to a four point probe was not possible so the resistance was calculated from a rougher two point probe method using a transmission line measurement. Contact resistance was backed out by taking a series of measurements at different distances. From our testing apparatus, the relationship between total resistance and sheet resistance for our nanowire mesh is:

$$R_t = R_s \left(\frac{L}{W} \right) + R_c$$

Where R_t is total resistance, R_s is sheet resistance, L/W is the ratio of length to width of the area measured between the two probes and R_c is total contact resistance. This was plotted on a graph where resistance versus length/width between the two probes was used. Using a particular sample not included in the rest of this thesis, the total contact resistance for the gold nanowire films was determined to be 24.53 ohms. This was subtracted from the total resistance of the nanowire meshes on flexible substrates and used to find sheet resistance. An R^2 value of .975 indicated that the values were very close to being linear indicating that the transmission line method could be used.

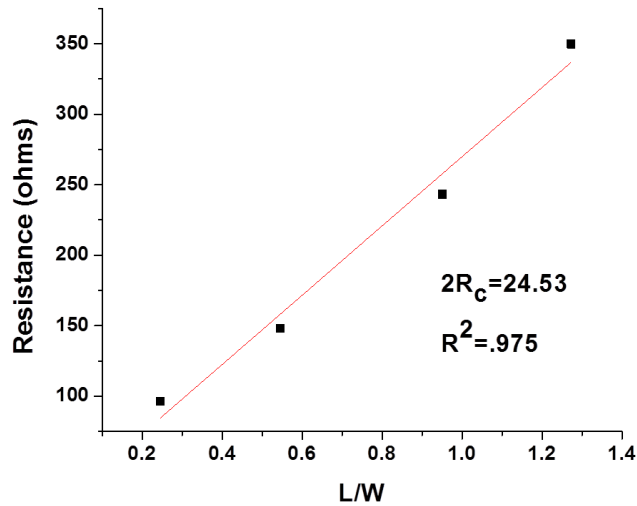


Figure 4.6: Transmission line measurement graph as an example used to calculate contact resistances.

For the devices on glass, the contact resistance was found to be much smaller between the tungsten tips and gold pads. Here, the contact resistance was found to be 2.6 ohms with an R^2 value of 1. This made sense as the contact resistance between the two metals should be low as a result of ohmic contact. Maximum force was used on the gold pad to keep contact resistance values the same for each distance tested. Contact resistance can be reduced significantly by applying maximum pressure from the probes.²² This was done on every sample to reduce contact resistance as much as possible.

4.3 Results and Discussion

4.3.1 Quality of gold coated silver nanowires

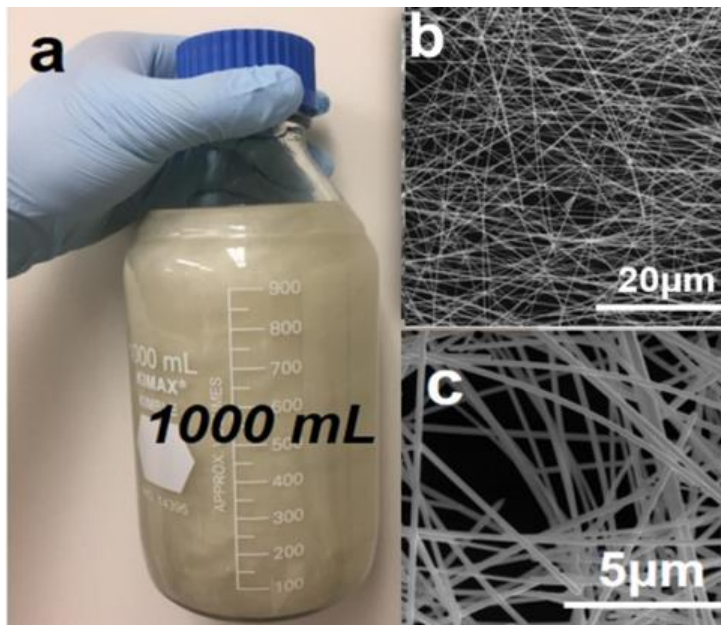


Figure 4.7: a) Silver nanowire solution produced in mass. b) Low magnification SEM image showing nanowires are quite long. c) Higher magnification SEM image.

The silver nanowires produced were ultra-long (greater than 100 microns) with an aspect ratio of around forty. Silver nanowires could be produced in mass, up to one thousand milliliter vials and were highly uniform in length. This was advantageous to the samples we were trying to create as it would limit the amount of junctions between nanowires for meshes that were not thick. SEM images revealed that the silver nanowires were not full of defects.

High resolution TEM revealed that the gold coating on the silver nanowires had a thickness of about six nanometers. In addition, EDS mapping confirmed the presence of gold coating on the outside of the silver nanowires. Such similar EDS profiles were obtained from numerous individual nanowires, indicating that galvanic etching was

avoided in synthesis. The suppression of galvanic etching leads to an atomically smooth, ultra-thin Au coating on the Ag surface. A line scan reveals that gold is conformably present across the surface of the silver nanowire. The nanowire itself used in these series of images was 180 nanometers in diameter.

It was also found under SEM that gold coated silver nanowires experienced no corrosion over a much longer period of time than the silver nanowires did. By day 21, the silver nanowires can clearly be seen as being sulfurized on the surface. By day 183, about six months after the start of the experiment, gold nanowires still do not show corrosive elements. However, it can be seen that some welding has occurred, possibly from ambient light.

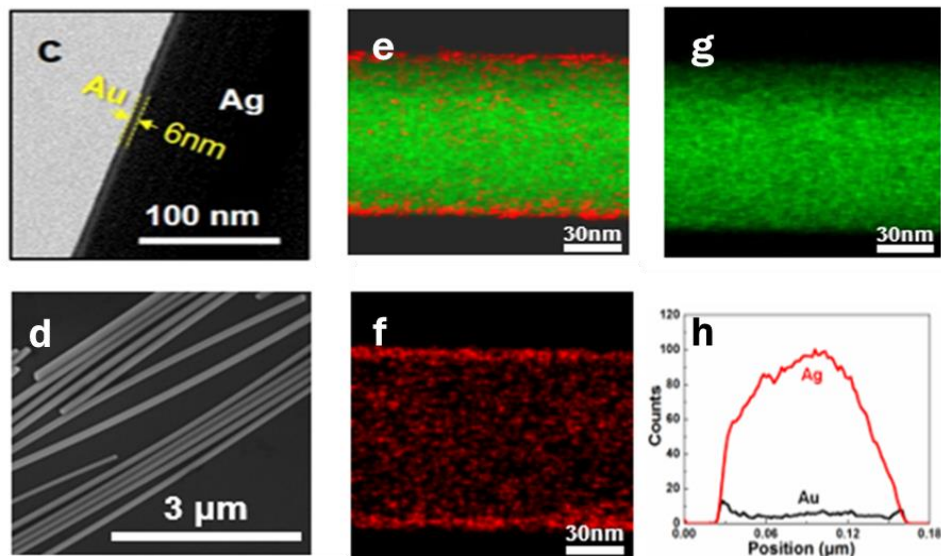


Figure 4.8: c) TEM image reveals 6 nm gold coating. d) SEM image of Ag@Au NWs. e,f,g) EDS mapping over a single Ag@Au NW (red is gold, silver is green) h) Line scan showing Au is present across the entire surface.

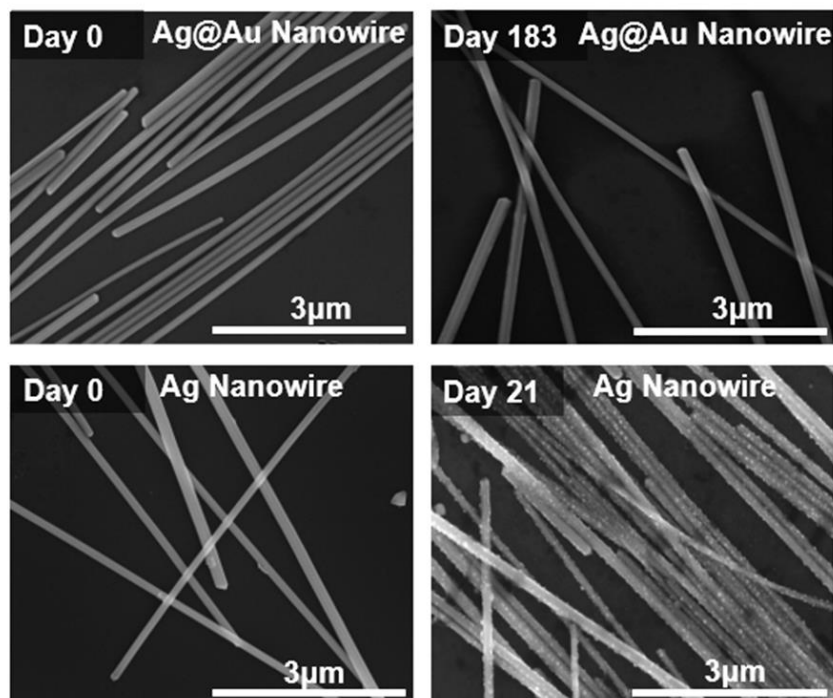


Figure 4.9: SEM images of Ag@Au NWs as compared to Ag NWs after being exposed to atmosphere.

4.3.2 Drop casting of silver nanowires onto flexible substrates

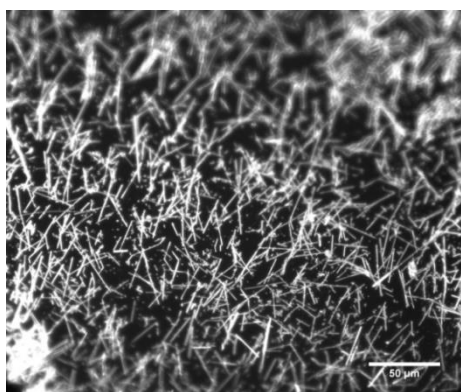


Figure 4.10: AgNWs dropcasted on glass substrate.

When nanowire networks were drop casted onto glass slides with electrodes, it was found that nanowires tended to form clumps that resulted in unusable samples. This was expected and prevented the formation of nanowire networks.¹⁶

Not a single working IV curve could be created using this method and matched up with literature which repeatedly stated that nanowire networks could not be created using this. Thus, it was revealed that another method needed to be used to create workable nanowire networks from our samples.

4.3.2 Plasmonic nanowire welding

Plasmonic nanowelding showed mixed results. SEM images after performing the nanowelding procedure showed that while it did work, it was not uniform and could even create breakages in some junctions. Irradiation times between 30 seconds and 30 minutes did not show much difference from each other and thus there was no way to optimize this method. This is in contrast to

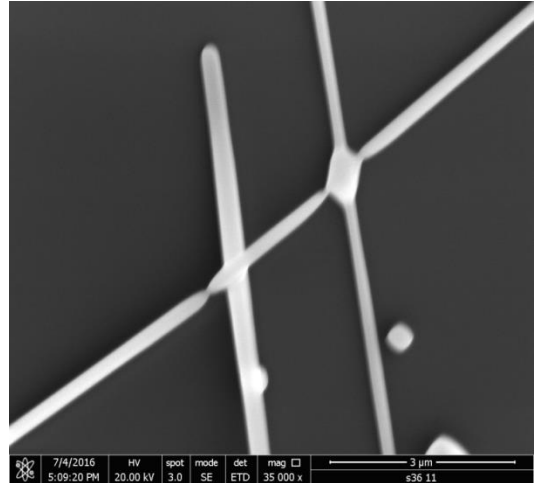


Figure 4.11: SEM image of AgNWs after plasmonic nanowire welding.

other literature reports which found even heating across their surface, even by the use of sunlight.¹⁶ It is thought that our samples received uneven heating not because of the quality of the nanowires but the heat effects from the incandescent bulb used which may have unevenly heat the surface. Unfortunately, this method was unusable. As stated, nanowire meshes were pressed onto substrates used in section 4.3.3 for resistance measurements.

4.3.3 Resistance measurements

Sheet resistance measurements for the nanowire meshes in condition 4 produced on PET substrates showed varying values versus level of transparency in the visible range. This range is important for the use of solar cells or electronic touch screens.²¹ The results did follow the expected trend that higher levels of transmittance over the visible range would lead to greater sheet resistance. Our values show that the press on filter method used is a simple yet not extraordinarily good method of producing gold

coated silver nanowire meshes as other literature have shown lower sheet resistance values for prepared nanowire meshes using silver nanowires and even ITO.³ Further methods are currently being developed in our lab that use roll to roll coating techniques that can decrease this sheet resistance even further.

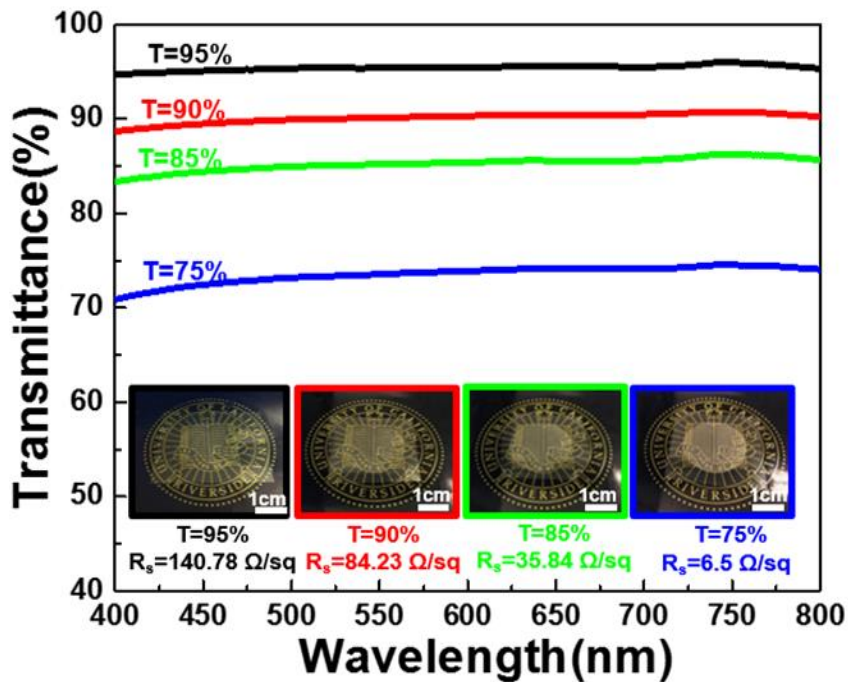


Figure 4.12: Transparency in the visible range for measured sheet resistances.

Resistance measurements revealed that overall, the gold coating around the silver nanowires prolonged the ability of the nanowire networks to produce a working electrode. The samples that used silver paste electrodes were the worst samples in terms of electrical performance over time. It was quickly shown that the silver paste used for the electrodes fell apart over time. This was actually to be expected as silver corrodes under atmospheric conditions. The silver paste started to interfere with the overall resistance measurements and prevented the network to be isolated as changing variable. Thus, data is not shown here for this condition as it was highly inaccurate.

The samples that remained in the 80 deg C oven without added humidity showed the predicted trend. The gold coated silver nanowires outperformed the silver coated nanowires by eighty-two days. The data was not recorded once the devices no longer produced readable current. It is believed that because the testing structures were the same that the only changed variable was the nanowire network itself. The silver nanowire network resistance started out at twenty eight ohms while the gold coated nanowire network started at twelve ohms. Though the silver nanowire sample started out

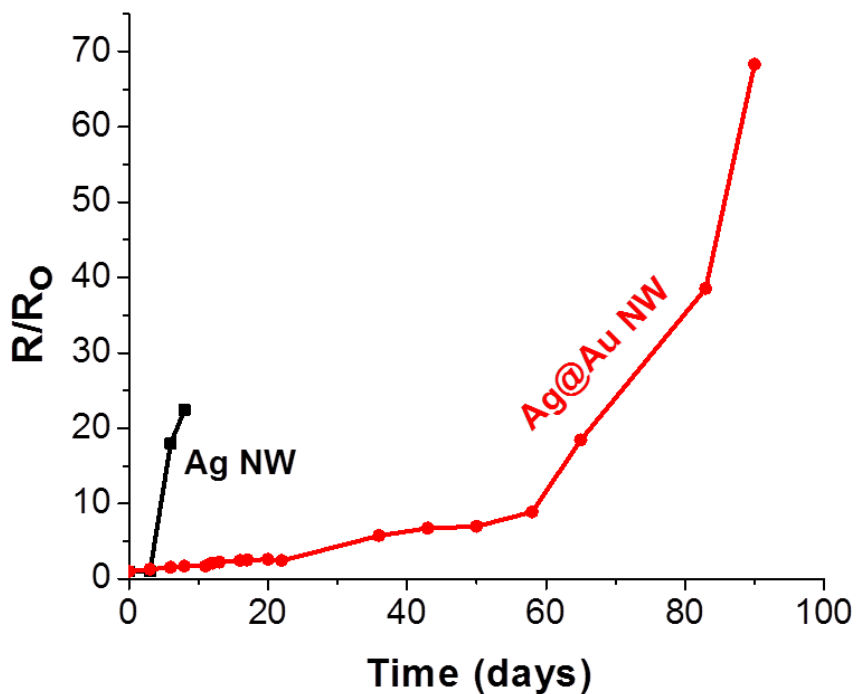


Figure 4.13: Comparing overall resistance to starting resistance (R/R_0) for nanowire meshes over time for 80 deg C condition.

at a slightly higher resistance, it quickly developed a much higher resistance than the gold coated silver nanowire network sample until the device was no longer usable.

The samples in the 100% humidity/80 deg C environment showed the greatest difference in performance between the two scenarios. It was found that the bare silver nanowires failed after just 45 days. However, the gold coated silver nanowire test is still on going. The original resistance of the silver nanowire network device was twenty ohms while that of the gold coated silver nanowire network is 7.6 ohms. The final resistance of the gold coated silver nanowire network is currently 7.8 ohms. Thus, there has been almost no change in the overall resistance.

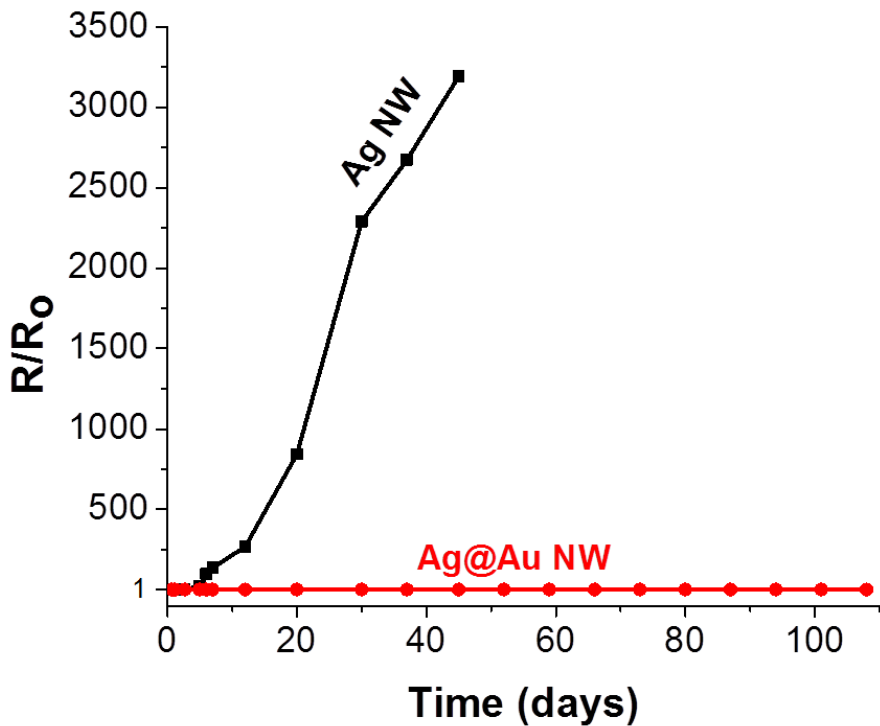


Figure 4.14 Comparing overall resistance to starting resistance (R/R_0) for nanowire meshes over time for 80 deg C condition.

It is interesting to find that the added humidity actually improved the nanowire networks. This is most likely because humidity assisted annealing probably occurred in this setting. Normally, annealing processes for nanowire networks occur best in dry environments at 140-250 deg C. However, humidity assisted annealing can occur as low as 45-60 deg C for humidity ranging from five to eighty percent relative humidity.²⁰

4.4 References

1. Yan R, Pausauskie P, Huang J, Yang P. "Direct photonic – plasmonic coupling and routing in single nanowires." *PNAS*. 2009;106(50).
2. Won J, Lee MY, Roy AK, Lee KS, Park SY. "Poly (dimethyl siloxane) -protected silver nanowire network for transparent conductor with enhanced oxidation resistance and adhesion properties." *Chem Lett*. 2013;191–3.
3. Ye S, Rathmell AR, Chen Z, Stewart IE, Wiley BJ. "Metal nanowire networks : the next generation of transparent conductors." *Adv Mater*. 2014;6670–87.
4. Cheong H, Triambulo RE, Lee G, Yi I, Park J. "Silver nanowire network transparent electrodes with highly enhanced flexibility by welding for application in flexible organic light-emitting diodes." *Appl Mat Inter*. 2014;
5. Gao C, Lu Z, Liu Y, Zhang Q, Chi M, Cheng Q. "Highly stable silver nanoplates for surface plasmon resonance biosensing" *Angewandte*. 2012;8:5629–33.
6. Liu H, Liu T, Zhang L, Han L, Gao C, Yin Y. "Etching-free epitaxial growth of gold on silver nanostructures for high chemical stability and plasmonic activity." *Mat Views*. 2015;5435–43.
7. Metraux GS, Cao YC, Jin RC, Mirkin CA. "Triangular nanoframes made of gold and silver." *Nano Lett*. 2003;3(4):519–22.
8. Xiong W, Liu H, Chen Y, Zheng M, Zhao Y, Kong X, et al. "Highly conductive, air-stable silver nanowire@iongel composite films toward flexible transparent electrodes." *Adv Mater*. 2016;7167–72.
9. Göbelt M, Keding R, Schmitt SW, Hoffmann B, Jäckle S, Latzel M, et al. "Encapsulation of silver nanowire networks by atomic layer deposition for indium-free transparent electrodes." *Nano Energy*. 2015;196–206.
10. Chou CY, Seo JH, Tsai YH, Ahn JP, Paek E, Cho MH, et al. "Anomalous stagewise lithiation of gold-coated silicon nanowires: a combined in situ characterization and first-principles study." *ACS Appl Mater Interfaces*. 2015;7(31):16976–83.
11. Hu L, Wu H, Cui Y. "Metal nanogrids, nanowires, and nanofibers for transparent electrodes." *MRS Bull*. 2011;36(October):760–5.
12. Aizenberg BP and J. "Calcite shape modulation through the lattice mismatch between the self-assembled monolayer template and the nucleated crystal face." *CrystEngComm* . 2007;9(12):1178.

13. Wiriyakun N, Pankhluab K, Boonrungsiman S, Laocharoensuk R. "Site-selective controlled dealloying process of gold-silver nanowire array: a simple approach towards long-term stability and sensitivity improvement of sers substrate." *Sci Rep* . 2016;6(1):39115.
14. Korte KE, Skrabalak SE, Xia Y. "Rapid synthesis of silver nanowires through a CuCl- or CuCl₂-mediated polyol process." 2008;437–41.
15. El Mel AA, Chettab M, Gautron E, Chauvin A, Humbert B, Mevellec JY, et al. "Galvanic replacement reaction: a route to highly ordered bimetallic nanotubes." *J Phys Chem C*. 2016;120(31):17652–9.
16. Kou P, Yang L, Chang C, He S. "Improved flexible transparent conductive electrodes based on silver nanowire networks by a simple sunlight illumination approach." *Sci Rep* . 2017;7(July 2016):42052.
17. José Andrés L, Fe Menéndez M, Gómez D, Luisa Martínez A, Bristow N, Paul Kettle J, et al. "Rapid synthesis of ultra-long silver nanowires for tailor-made transparent conductive electrodes: proof of concept in organic solar cells." *Nanotechnology* . 2015;26(26):265201.
18. Angmo D, Andersen TR, Bentzen JJ, Helgesen M, Sundergaard RR, Jorgensen M, et al. "Roll-to-roll printed silver nanowire semitransparent electrodes for fully ambient solution-processed tandem polymer solar cells." *Adv Funct Mater*. 2015;25(28):4539–47.
19. Garnett EC, Cai W, Cha JJ, Mahmood F, Connor ST, Greyson Christoforo M, et al. "Self-limited plasmonic welding of silver nanowire junctions." *Nat Mater* . 2012;11(3):241–9.
20. Weiß N, Müller-Meskamp L, Selzer F, Bormann L, Eychmüller A, Leo K, et al. "Humidity assisted annealing technique for transparent conductive silver nanowire networks." *RSC Adv* . 2015;5(25):19659–65.
21. Nanowire S, Hu L, Kim HS, Lee J, Peumans P, Cui Y. "Scalable coating and properties of transparent ag nanowire." *ACS Nano*. 2010;4(5):2955–63.
22. Das AJ, Shivanna R, Narayan KS. "Photoconductive nsom for mapping optoelectronic phases in nanostructures." *Nanophotonics*. 2014;3(1–2):19–34.
23. Bellew AT, Manning HG, Gomes da Rocha C, Ferreira MS, Boland JJ. "Resistance of single ag nanowire junctions and their role in the conductivity of nanowire networks." *ACS Nano*. 2015;9(11):11422–9.

Chapter 5

Conclusions

5.1 Summary

We were able to move research forward on two fundamental problems related to the advancement of flexible electronics, the reduction of contact resistance in 2H MoS₂ based devices, and the protection of flexible silver nanowire networks from atmospheric corrosion for flexible electronics. Large area single layer MoS₂ was synthesized by chemical vapor deposition using a repeatable, developed process. It was found that by adjusting for such parameters as flow rate, precursor amount, temperature of synthesis (ramping and final), pressure and boat configuration, that a stable process for single layer domains could be achieved creating domains between 15 to 70 microns in diameter. The quality of the MoS₂ was observed using Raman spectroscopy, photoluminescence measurements, and atomic force microscopy. Raman spectroscopy revealed that the samples were single layer from their two major optical modes E¹_{2g} and A_{1g}. Photoluminescence measurements with a small FWHM indicated the sample was highly crystalline and of good quality. Finally, AFM measurements further confirmed a height of about .7 nm indicating the samples were monolayer with no obvious defects. This MoS₂ could be transferred to a series of surfaces including flexible PDMS, gold and glass by using a simple water based method and their structure remained intact.

In order to reduce contact resistance in MoS₂ based devices, a new mechanism was proposed for using a benign, out of the glove box, photochemically based synthesis. This mechanism relied on the use of a photochemical method involving excitation of

single layer MoS₂ using a 532 nm laser in a solution of 1M LiPF₆ in propylene carbonate. We placed samples of single layer MoS₂ in this solution and confirmed the presence of partial phase change using Raman spectroscopy and XPS analysis. We then did 2D mapping of the photoluminescence to try to show change across the entire domain and confirmed with AFM that although there was a drop in photoluminescence as expected, there was no obvious damage to the domain itself. We then did a series of control experiments to see if we would get the same effect using just propylene carbonate, LiPF₆ in acetonitrile, or using a 785 nm laser. As predicted, none of these methods worked as well as using a 532 nm laser with Li⁺ present as a stabilization agent. We also found a rough power dependency relationship with the time at which phase change occurred but because of inconsistency in the samples, we couldn't find a relationship past this. Unfortunately, as a result of difficulties with the photolithography procedure to make devices using 1T phase MoS₂, only a preliminary device could be made. In addition, a device was created to test phase change through purely electrochemical means but failed to produce equivalent results.

In order to protect silver nanowires from atmospheric corrosion and make them usable for flexible electronics, we developed a solution based method for coating them with gold that overcame galvanic replacement. These nanowires were ultra-long (>100 microns) and conformably coated with gold. We first confirmed this actually occurred using HR-TEM, SEM and EDS mapping to find a coating of six nanometers was developed. We then developed a method for creating nanowire meshes out of this solution in three different scenarios by using a press on filter method. The first scenario on a flexible substrate did not have usable data because of interference from the silver

paste contacts. The resistance values results over time revealed that the gold covered nanowires outperformed the bare silver nanowires in the 80 deg C and 80deg C/100% humidity test scenarios as expected. Transparency in the visible range relative to the overall sheet resistance was calculated as well.

5.2 Suggestions for future work

The work contained in this thesis were preliminary works that advanced new fields of scientific study and are really just the start of collecting information concerning these topics. Our individual MoS₂ domains, while good for testing fundamental physics, are not the best size for large scale device fabrication. More reliable or refined methods must be developed for creating large area monolayers on the millimeter scale. At least, individual monolayer islands of dimensions two hundred by two hundred microns should be created to match more traditional photolithography masks and tools used to make devices. Also, these procedures should be developed for flexible substrates such as PET or PDMS without the need for transfer if possible.

In regards to the photochemical phase change project, there is a lot of further investigation that needs to be done into what parameters actually encourage the phase change to occur. Samples produced using CVD are inherently non-uniform and thus different types and amounts of point defects may contribute to exciton travel throughout the system. A relationship needs to be developed between the number of defects in a MoS₂ monolayer and the time at which phase change occurs across that surface using such techniques as high resolution TEM. In addition, parameters such as laser spot size, amount of redox species, amount of stabilizing Li⁺ ion, temperature and layers of MoS₂ must all be looked at in relation to the time at which phase change occurs.

It is believed that this process should work for other TMDs such as WS_2 or MoSe_2 who have similar band gaps and valence band/conduction band positions. This process should be extended to those TMDs to see if there is potential for a universal process of photochemical phase change or even the possibility of heterostructures that incorporate a new 1T phase. Finally, devices made out of the 1T MoS_2 at the contacts must be created and tested for characteristics such as on/off ratio, subthreshold swing, and electron/hole mobility values. These must then be compared to similarly made devices using 2H phase MoS_2 .

Currently, there is further work being done on the nanowire networks in our group. This research includes looking at the mechanical stability of the gold coated silver nanowire networks under mechanical flexing. Also, we are currently working on a method of developing a spray on process for gold coated silver nanowire networks to reduce the number of contact points between wires, thus reducing the overall resistance. Copper nanowires are being created as an alternative to the silver nanowire networks and they are being tested for their stability in open air as well. These will be formed into nanowire networks and compared to their gold coated silver nanowire counterparts. Finally, it remains to be seen how metal nanowire networks when used in practical devices will stand up against more traditional electrodes like ITO. There is the possibility for long lasting flexible devices using materials like 1T MoS_2 or metal nanowire networks but there is still a lot of work to do to develop these concepts on the commercial scale.